





Experimental and theoretical investigation of the thermal effect in the Casimir interaction from graphene

M. Liu,¹ Y. Zhang ¹, G. L. Klimchitskaya ^{2,3}, V. M. Mostepanenko ^{2,3,4} and U. Mohideen ^{1,*}

¹*Department of Physics and Astronomy, University of California, Riverside, California 92521, USA*

²*Central Astronomical Observatory at Pulkovo of the Russian Academy of Sciences, Saint Petersburg, 196140, Russia*

³*Institute of Physics, Nanotechnology and Telecommunications, Peter the Great Saint Petersburg Polytechnic University, Saint Petersburg, 195251, Russia*

⁴*Kazan Federal University, Kazan, 420008, Russia*



(Received 3 June 2021; accepted 16 August 2021; published 27 August 2021)

We present the results of an experiment on measuring the gradient of the Casimir force between an Au-coated hollow glass microsphere and graphene-coated fused silica plate by means of a modified atomic force microscope cantilever-based technique operated in the dynamic regime. These measurements were performed in high vacuum at room temperature. The energy gap and the concentration of impurities in the graphene sample used have been measured utilizing scanning tunneling spectroscopy and Raman spectroscopy, respectively. The measurement results for the gradients of the Casimir force are found to be in a very good agreement with theory using the polarization tensor of graphene at nonzero temperature depending on the energy gap and chemical potential with no fitting parameters. The theoretical predictions of the same theory at zero temperature are experimentally excluded over the measurement region from 250 to 517 nm. We have also investigated a dependence of the thermal correction to the Casimir force gradient on the values of the energy gap, chemical potential, and on the presence of a substrate supporting the graphene sheet. It is shown that the observed thermal effect is consistent in size with that arising for pristine graphene sheets if the impact of real conditions such as nonzero values of the energy gap, chemical potential, and the presence of a substrate is included. Implications of the obtained results to the resolution of the long-standing problems in Casimir physics are discussed. In addition to the paper published previously [M. Liu *et al.*, *Phys. Rev. Lett.* **126**, 206802 (2021)], we present measurement results for the energy gap of the graphene sample, double the experimental data for the Casimir force, and perform a more complete theoretical analysis.

DOI: [10.1103/PhysRevB.104.085436](https://doi.org/10.1103/PhysRevB.104.085436)

I. INTRODUCTION

An investigation of different effects in graphene brought to light that this material possesses a variety of unusual properties which are of much interest to fundamental physics. It is well known that graphene is characterized by a minimum electrical conductivity and low absorbance expressed in terms of fundamental constants [1–4] and provides possibilities for experimentally testing the Klein paradox [5], the effect of Schwinger pair creation from vacuum in external electric field [6–9], and the relativistic quantum Hall effect [10]. This is a consequence of graphene being a two-dimensional material which at low energies is well described not by the Schrödinger equation but by the relativistic Dirac equation where the speed of light c is replaced by the much lower Fermi velocity v_F [11–13].

One of the challenging problems is the experimental and theoretical investigation of the thermal Casimir interaction in graphene systems. The Casimir force [14] is the relativistic generalization of a more familiar van der Waals force. This is an entirely quantum phenomenon which originates from

the zero-point and thermal fluctuations of the electromagnetic field whose spectrum is altered by the presence of material boundaries, no matter be they three- or two-dimensional. The fundamental unified theory of the van der Waals and Casimir forces was created by Lifshitz [15,16]. In the framework of this theory, the Casimir free energy and force are expressed via the reflection coefficients of electromagnetic fluctuations on the boundary surfaces. In the original formulation, only the plane boundaries were considered but currently the Lifshitz theory is generalized to the case of arbitrarily shaped bodies [17–21].

Precise measurements of the thermal Casimir force between metallic test bodies using the present-day laboratory techniques revealed a puzzling problem. In many experiments performed by different experimental groups, it was found that the predictions of the Lifshitz theory come into conflict with the measurement data if the much-studied relaxation properties of conduction electrons at low frequencies are taken into account in computations [22–34] (see also monograph [35] and reviews [36–38]). Note that in Ref. [39] an agreement was obtained by subtracting a hypothetical electrostatic force between a centimeter-size spherical lens and a plate which was ten times larger than the Casimir force. This result, however, ignored imperfections of the lens surface which have an

*Umar.Mohideen@ucr.edu

important effect on the measured force [40]. What is even more surprising, an agreement between experiment and theory is restored if computations are performed with simply discarded relaxation properties of conduction electrons [22–38]. Specifically, experiments using magnetic metal surfaces [27–29] and isoelectronic difference force measurements [30] have reconfirmed this conclusion with an extraordinary precision.

It should be emphasized that the reflection coefficients used in the standard Lifshitz theory are expressed via the dielectric permittivities of boundary materials which in turn are found from the available optical data for the complex index of refraction [41] extrapolated down to zero frequency. The best-known method for extrapolation is by means of the Drude model. Under certain assumptions, this model can be derived from Boltzmann transport theory or the Kubo formula and finds full verification in the area of electromagnetic phenomena other than the Casimir effect [42]. The Drude model takes proper account of the relaxation properties of conduction electrons in metals by means of the temperature-dependent relaxation parameter. However, the Lifshitz theory using the Drude model predicts a relatively large thermal effect in the Casimir force at short separation distances [43] which was excluded by the experiments mentioned above.

Graphene provides great advantages for the resolution of this problem. The point is that at energies below a few electron volts characteristic for the Casimir force at separations exceeding 100 nm, graphene can be considered in the framework of the Dirac model as a set of massless or very light electronic quasiparticles. The response function of such a simple system to the electromagnetic field can be found on the basis of the first principles of quantum electrodynamics at nonzero temperature without resort either to phenomenological approaches or simplified models.

There is an extensive literature on the theory of the Casimir interaction in graphene systems using the Kubo formalism, density-density correlation functions, two-dimensional Drude, and other models [44–61]. Specifically, using the formalism of correlation functions in the random phase approximation, which is ultimately equivalent to the Lifshitz theory, Gómez-Santos predicted a large thermal effect in the Casimir interaction between two parallel graphene sheets even at separations of tens of nanometers at room temperature [45]. This prediction relates to an order of magnitude shorter separations compared to the thermal effect between metallic plates predicted using the Drude model which was already excluded experimentally [22–38].

The question arises on whether or not an unusually big thermal effect exists for graphene. This question should be answered both theoretically and experimentally. Rigorous theoretical description of the Casimir interaction in graphene systems is based on the Lifshitz theory supplemented by the response function of graphene to quantum fluctuations. The latter is given by the polarization tensor of graphene which can be found in the framework of the Dirac model (see, e.g., Ref. [62]).

Real graphene sheets are characterized by some value of the chemical potential, which depends on the concentration of impurities, and of the energy gap which is caused by structural defects, impurities, interelectron interactions, and the pres-

ence of a substrate [12,13]. The exact polarization tensor of graphene at zero temperature was found in Ref. [63] and at nonzero temperature in Ref. [64] (the latter results are valid only at the pure imaginary Matsubara frequencies). The exact expressions for the polarization tensor of gapped graphene valid over the entire plane of complex frequencies, including the real frequency axis, was found in Ref. [65] and generalized for the case of nonzero chemical potential in Ref. [66].

The formalism of the polarization tensor was used to investigate the thermal Casimir and Casimir-Polder forces in graphene systems [67–80]. Specifically, in Ref. [69] it was shown that the polarization tensor leads to more exact results than several phenomenological approaches used in the literature. According to the results of Ref. [76], the formalisms of the polarization tensor and of the density-density correlation functions are eventually equivalent. In fact, from the exact components of the polarization tensor it has been possible to find the respective density-density correlation functions at nonzero temperature which were not known until then. Most importantly, calculations using the polarization tensor confirmed [69,77] the prediction of an unusually big thermal effect in the Casimir force from graphene at short separations [45]. Thus, an experimental discovery of this interesting effect has assumed great importance for both fields of graphene and Casimir research.

The first experiment on measuring the Casimir force between an Au-coated sphere and a graphene-coated SiO₂ film deposited on a Si substrate was performed using an atomic force microscope (AFM)-based technique operated in the dynamic regime [81]. The measurement results were found in good agreement with theory using the polarization tensor of graphene [82]. Because of the thin SiO₂ film used, it was not possible, however, to separate the unusual thermal effect from the total force gradient. According to Ref. [74], observation of the thermal effect from graphene would become possible by increasing the thickness of an underlying SiO₂ film.

Using this approach, the thermal Casimir interaction from graphene was recently measured in the configuration of an Au-coated sphere and a graphene sheet deposited on thick SiO₂ substrate [83]. The measured gradients of the thermal Casimir force were found to be in a very good agreement with theoretical predictions calculated using the polarization tensor accounting for the chemical potential of graphene determined by means of Raman spectroscopy. An estimated range of the energy gap values was included as a part of the theoretical error. By comparing with respective theoretical results at zero temperature, an unusual thermal effect from graphene was reliably demonstrated over the separation region between a sphere and a graphene sheet from 250 to 590 nm at room temperature.

In this paper, we present additional experimental information and a more complete theoretical analysis regarding the experiment on measuring the thermal Casimir interaction from graphene. While the conclusions made in Ref. [83] were based on one measurement set consisting of 21 runs with a step in separation distances of 1 nm, we have now performed the second measurement set and made an averaging procedure over a more representative wealth of evidence which includes 42 runs. Another important innovation is that the value of the energy gap for a graphene sample used in the experiment

was measured by means of scanning tunneling spectroscopy. As a result, it has been possible to compute the theoretical force gradients using the polarization tensor with the definite values of both the chemical potential and the energy gap of graphene rather than include an estimated range of the energy gap values in the theoretical error as was done in Ref. [83]. Although the measured value of the energy gap turned out to be somewhat outside the range estimated in Ref. [83], we have clearly confirmed the presence of an unusual thermal effect in the graphene sample used within the separation region from 250 to 517 nm.

On the theoretical side, we have performed calculations elucidating the physical nature of the unusually big thermal effect in the Casimir interaction from graphene at short separations and its dependence on the chemical potential, energy gap, and the presence of a substrate for real graphene samples. The case of a pristine graphene was also considered. A comparison between experiment and theory was made on the basis of first principles of quantum electrodynamics at nonzero temperature with no fitting parameters and a very good agreement was demonstrated. Implications of the obtained results to a long-standing problem of the thermal Casimir force between metallic test bodies are discussed.

The paper is organized as follows. In Sec. II, we consider the experimental procedures used for measuring the gradient of the Casimir force between an Au-coated sphere and a graphene-coated SiO₂ substrate. Section III describes measurements of the impurity concentration and energy gap in the experimental graphene sample. In Sec. IV, theory of the Casimir interaction using the polarization tensor of graphene is briefly considered in application to the experimental configuration. In Sec. V, we calculate the magnitude of the unusually big thermal effect in different graphene systems and elucidate its physical nature. Section VI contains the comparison between experiment and theory. In Sec. VII, the reader will find our conclusions and a discussion of the obtained results and their implications.

II. MEASURING THE CASIMIR FORCE GRADIENT FROM GRAPHENE USING A CUSTOM ATOMIC FORCE MICROSCOPE CANTILEVER-BASED SETUP IN THE DYNAMIC REGIME

Measurements of the gradient of the Casimir force between an Au-coated hollow glass microsphere and a graphene-coated fused silica glass (SiO₂) plate have been performed by means of a custom-built AFM cantilever-based technique operated in the dynamic regime at a temperature $T = 294.0 \pm 0.5$ K in high vacuum below 9×10^{-9} Torr. Similar setups have already been used in previous experiments on measuring the gradient of the Casimir force between metallic surfaces [26–29,31–33] (the schematic can be found in Fig. 1 of Ref. [33] but here the UV- and Ar-ion cleaning is not used to avoid damaging the graphene sheet). Below we consider only the most important features connected with the use of graphene sample.

The main test body in this experiment was made from a large-area graphene sheet which was chemical vapor deposition grown on a Cu foil [84]. This sheet was transferred onto a polished JGS2 grade fused silica double side optically

polished substrate of 10-cm diameter and 0.05-cm thickness [85]. This was made through an electrochemical delamination procedure [84,86]. Then a 1×1 cm² piece of the graphene-coated fused silica substrate was cut from the entire sample and used as the test body in measuring the force gradient. After the force gradient measurements have been performed, the rms roughness of the graphene sheet on a fused silica substrate was measured to be $\delta_g = 1.5 \pm 0.1$ nm by means of an AFM. This is used in Sec. VI for comparison between experiment and theory.

The second test body is an Au-coated hollow glass microsphere with the diameter $2R = 120.7 \pm 0.1$ μm measured by means of a scanning electron microscope. In doing so, the thickness of Au coating was measured to be 120 ± 3 nm using an AFM. After the experiment was completed, the rms roughness of the Au coating on the sphere $\delta_s = 0.9 \pm 0.1$ nm was measured by means of an AFM.

A hollow glass microsphere is attached to the end of an Au-coated tipless AFM cantilever using silver epoxy and then coated with Au [87]. Before attaching the sphere and Au coating, the cantilever spring constant was reduced through chemical etching (see Ref. [33] for details). As a result, the corresponding resonant frequency of the cantilever was decreased from 5.7579×10^4 to 3.5286×10^4 rad/s by etching in 60% potassium hydroxide solution at 75 °C with stirring for 100 s. Note also that, prior to etching, the cantilever was washed in a buffered oxide etch solution and deionized water for 1 min each. After the Au coating, the resonant frequency of the complete cantilever-sphere system in vacuum was measured to be $\omega_0 = 6.1581 \times 10^3$ rad/s.

The vacuum chamber containing the cantilever-sphere system and graphene sample on a fused silica substrate was pumped using an oil-free scroll pump and then followed by a turbo pump connected in series, and finally an ion pump for further pressure reduction. During the force measurements, only the ion pump was used, thereby reducing the mechanical vibrations (see Refs. [26,31–33] for details). In the dynamic measurement regime used, the cantilever with the attached sphere was set to oscillate above the graphene plane. The oscillation frequency of the cantilever and movement of the graphene sample were monitored by two fiber interferometers with laser light sources of 1550 and 500.1 nm wavelength, respectively. Small changes in the separation distance between sphere and graphene due to mechanical drift during the measurement were monitored and corrected as described in Refs. [26,32,33]. The frequency shifts of the cantilever oscillation induced by any external force (electric or Casimir) were recorded using a phase lock loop (PLL) [26]. To stay in the linear regime, the oscillation amplitude of the cantilever was maintained at 10 nm, and the resolution of the PLL was measured to be 55.3 mrad/s.

The total force acting on the sphere is given by

$$F_{\text{tot}}(a, T) = F_{\text{el}}(a) + F(a, T). \quad (1)$$

Here, F_{el} is the electric force caused by the constant voltages V_i applied to the graphene sheet using ohmic contacts while the sphere remains grounded and by the residual potential difference V_0 , $F(a, T)$ is the Casimir force, a is the separation distance between the sphere and graphene sheet, and T is the temperature.

Under the influence of an external force (1), the resonant frequency ω_0 of the cantilever-sphere system is modified to $\omega_r(a, T)$ and the frequency shift

$$\Delta\omega(a, T) = \omega_r(a, T) - \omega_0 \quad (2)$$

was recorded by the PLL at every 0.14 nm while the graphene-coated fused silica plate was moved by the piezo actuator toward the sphere starting at the maximum separation. Using interpolation, the values of $\Delta\omega$ can be recalculated with a step of 1 nm. We recall that all measurements were performed at constant $T = 294$ K. The argument T in the Casimir force is discussed during comparison with the theory in Secs. IV–VI.

In the linear regime, the frequency shift (2) is given by [26,88]

$$\Delta\omega(a, T) = -CF'_{\text{tot}}(a, T) = -CF'_{\text{el}}(a) - CF'(a, T). \quad (3)$$

Here, the calibration constant $C = \omega_0/(2k)$, k is the spring constant of the cantilever, and the gradient of the electrostatic force in a sphere-plate geometry is given by [26,35]

$$F'_{\text{el}}(a) = X'(a, R)(V_i - V_0)^2, \\ X'(a, R) = \frac{2\pi\epsilon_0}{\sqrt{a(2R+a)}} \sum_{n=1}^{\infty} \text{csch}(n\tau) \{n \coth(n\tau) \\ \times [n \coth(n\tau) - \coth \tau] - \text{csch}^2 \tau + n^2 \text{csch}^2(n\tau)\}, \quad (4)$$

where $\cos \tau \equiv 1 + a/R$, ϵ_0 is the permittivity of vacuum, and the absolute separations between the zero levels of roughness on the sphere and graphene surfaces are determined from

$$a = z_{\text{piezo}} + z_0, \quad (5)$$

where z_{piezo} is the distance moved by the graphene-coated plate and z_0 is the closest separation between this plate and the sphere.

As a result, the gradients of the Casimir force can be expressed using Eq. (3) via the measured frequency shift

$$F'(a, T) = -\frac{1}{C} \Delta\omega(a, T) - F'_{\text{el}}(a), \quad (6)$$

where all the necessary parameters, C , z_0 , and V_0 , are determined by means of electrostatic calibration which is performed simultaneously with measurements of the frequency shifts (see Refs. [26,35] for details).

For this purpose, in the first measurement set reported in Ref. [83], ten different voltages from 0.083 V to 0.183 V with a step 0.01 V but with exception of 0.133 V and 11 voltages equal to 0.133 V were applied to the graphene sheet. At each separation a between the graphene-coated plate and the sphere 21 values of the frequency shift $\Delta\omega$ were measured and the value of V giving the maximum in the parabolic dependence of $\Delta\omega$ on V_i in Eqs. (3) and (4), determining the value of V_0 , was found with the help of a χ^2 -fitting procedure. Using the same fit, from the curvature of the parabola mentioned above, we have determined the values of z_0 and C . In Fig. 1(a), taken from Ref. [83], the obtained values of V_0 are shown as the function of separation between a sphere and a graphene-coated plate for the first measurement set. To check that the obtained values of V_0 do not depend on separation, we have performed the best fit of V_0 to the straight line $V_0 = d + \theta a$, where a is measured in nanometers, and

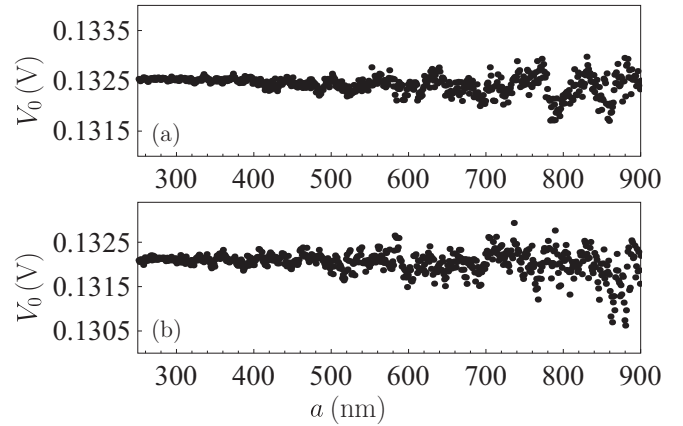


FIG. 1. The residual potential difference between an Au-coated sphere and a graphene-coated fused silica plate is shown by the dots as a function of separation (a) for the first and (b) second measurement sets.

found that $d^{(1)} = 0.1326$ V and $\theta^{(1)} = -2.73 \times 10^{-7}$ V/nm [83]. This demonstrates an independence of V_0 on a in this set of measurements up to a high precision. The mean value of V_0 in the first measurement set was $V_0^{(1)} = 0.1324$ V.

In a similar way, the values of z_0 and C were determined from the fitting procedure at each separation and found to be separation-independent, leading to the mean values $z_0^{(1)} = 236.9 \pm 0.6$ nm and $C^{(1)} = (4.599 \pm 0.003) \times 10^5$ s/kg.

As mentioned above, at each separation the frequency shift $\Delta\omega$ was measured for 21 times with different applied voltages. The respective experimental values of the gradient of the Casimir force were calculated by Eq. (6) and their mean values $F'_{(1)}(a, T)$ were found with a step of 1 nm. The random errors of these mean values were determined at the 67% confidence level. The systematic errors, which are mostly caused by the errors in measuring the frequency shift indicated above, were combined in quadrature with the random errors resulting in the total experimental errors of the first measurement set $\Delta_{\text{expt}}^{(1)} F'(a, T)$. The error in measuring the absolute separations was found to be $\Delta a = 0.6$ nm.

In addition to the first measurement set reported in Ref. [83], second set of measurements was performed with the same graphene sample, applied voltages, and using the same experimental procedures. This resulted in values of the residual potential difference shown in Fig. 1(b) as a function of separation. The best fit of these values to straight line results in $d^{(2)} = 0.1322$ V and $\theta^{(2)} = -3.41 \times 10^{-7}$ V/nm. The obtained parameters are only slightly different from those in the first set of measurements and again demonstrate an independence of the residual potential difference on separation. In the second measurement set, the mean value of V_0 was determined to be $V_0^{(2)} = 0.1320$ V.

The values of the separation on contact and the calibration constant in the second measurement set were also found to be independent of separation resulting in the following mean values: $z_0^{(2)} = 238.8 \pm 0.5$ nm and $C^{(2)} = (4.712 \pm 0.003) \times 10^5$ s/kg.

The independence of the residual potential difference on the sphere-graphene separation in both measurement sets

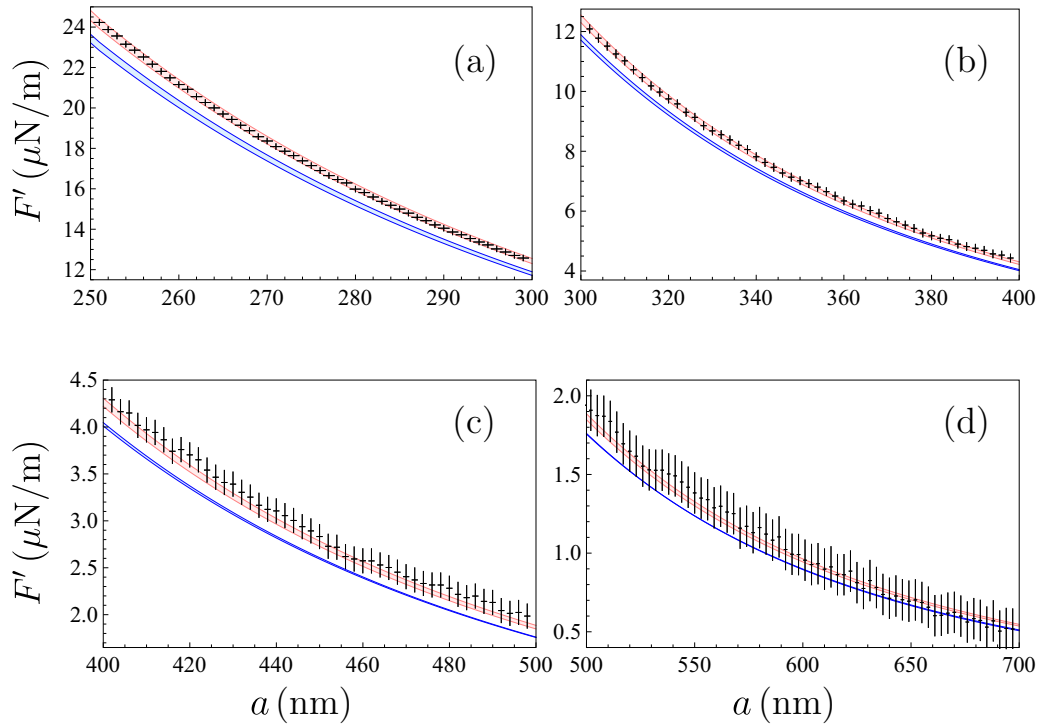


FIG. 2. The mean gradient of the Casimir force obtained from the two measurement sets is shown by the crosses as a function of separation within four separation intervals. The upper and lower theoretical bands are computed at the laboratory temperature $T = 294$ K and at $T = 0$ K, respectively (see the text for further discussion).

confirms that in this experiment performed in high vacuum the role of patch potentials on an Au-coated sphere and of spurious electrostatic interactions induced by charges on the SiO_2 substrate supporting graphene is negligibly small for the separations reported here. A similar situation holds for the experiments [22–34] performed in high vacuum with two Au or Ni-coated test bodies where a smallness of the electrostatic effects was confirmed by independent measurements employing Kelvin-probe microscopy [89]. Note that the graphene sheet is connected to a power supply which is a reservoir for compensating charges. As the graphene sheet is a two-dimensional conducting layer with high conductivity determined by the very light Dirac quasiparticles, which is connected to a power supply, it effectively screens out the role of possible charges on the SiO_2 substrate. This is confirmed by the measurements of mean impurity concentration in graphene presented in Sec. III. By contrast, the cases, where the role of patch effects can be relatively large, are considered in the experiments of Ref. [90] performed in ambient air with 30% relative humidity.

These results were used to find the experimental values of the gradients of the Casimir force at each separation and their mean $F'_{(2)}(a, T)$ with a step of 1 nm. Following the same procedure as described above, the total experimental errors in the second measurement set $\Delta_{\text{expt}}^{(2)} F'(a, T)$ were determined.

In each measurement set, the total experimental error is mostly determined by the systematic error which is almost the same for both sets. In doing so, an advantage of using the two sets of measurements is in the decreased impact of possible accidental systematic deviations.

Finally, we have calculated the experimental gradients of the Casimir force, $F'_{\text{expt}}(a, T)$, by averaging the mean values obtained in two measurement sets. In a similar way, the total experimental error of the measured gradients, $\Delta_{\text{expt}} F'(a, T)$, was obtained by averaging the total experimental errors found in the first and second measurement sets.

The measurement results for $F'_{\text{expt}}(a, T)$ obtained from the two sets of measurement are shown as crosses in Figs. 2(a)–2(d) over the separation range from 250 to 700 nm. The vertical and horizontal arms of the crosses have the lengths $2\Delta_{\text{expt}} F'(a, T)$ and $2\Delta a$, respectively, determined by the total experimental errors. For visual clarity, we have indicated all data points in Fig. 2(a), each second data point in Figs. 2(b) and 2(c), and each third data point in Fig. 2(d). The top and bottom bands indicated in Fig. 2 refer to the comparison between experiment and theory which is discussed in Sec. VI. Note that the minimum separation distance of 250 nm chosen in the experimental data reported here is typical for measurements of the Casimir force by means of an AFM in the dynamic mode [26–29,31–33]. This is done to not enter a nonlinear regime of the oscillator system used. On the theoretical side, the relative thermal effect in the Casimir interaction from graphene becomes more sensible just at $a > 250$ nm (see below in Sec. V, Fig. 6).

III. MEASUREMENTS OF THE IMPURITY CONCENTRATION AND ENERGY GAP OF GRAPHENE SHEET DEPOSITED ON A FUSED SILICA SUBSTRATE

It is well known that real graphene sheets are characterized by some small but nonzero mass of electronic quasiparticles

which leads to the presence of an energy gap Δ in their spectrum [12,13]. In a similar manner, real graphene samples contain some fraction of impurities and, as a result, are characterized by some nonzero chemical potential μ [12,13]. For pristine graphene sheets, it holds $\Delta = \mu = 0$. One should know the values of both the energy gap and chemical potential to calculate the response of a graphene sample to electromagnetic fluctuations. Because of this, it is desirable to determine both of them before comparing measurement results of the Casimir interaction in graphene systems with theoretical predictions.

We begin with determining the value of the chemical potential which is caused by the concentration of impurities. The impurity concentration in the graphene sample was determined using Raman spectroscopy after the measurement of the Casimir force gradient. The Raman spectroscopy was carried out using a Horiba Labram HR 800 system with 532-nm laser excitation (Laser Quantum, 65 mW power). A 100x objective lens with NA = 0.9, which renders a laser spot size of $0.4 \mu\text{m}^2$ and corresponding spot diameter of 709 nm was used. The measurements were done at a temperature of 294 ± 0.5 K. The spectrometer used a grating with 600 lines/mm to ensure the spectral range from 1450 cm^{-1} to 2900 cm^{-1} which includes both G and $2D$ peaks of graphene. The spectral resolution was maintained at 2 cm^{-1} for the precise detection of the G peak blueshift. The spectra were collected at 18 equidistant points on the sample to understand the spatial distribution of the impurity concentration. Prior to acquiring the spectra, to ensure that the sample was positioned at the focal plane, the signal intensity was maximized by adjusting the focus of the microscope. The spectra collected at each point are the accumulated results over ten acquisitions with each acquisition spanning over 10 s.

The G -peak spectra were fitted to a Lorentzian to identify the precise location of the peak. The values of the G peak were compared to G -peak shifts modified by charge concentration that are reported in Ref. [91] and the corresponding impurity concentration was identified as shown in Fig. 3. Here, the solid triangles are the data from Ref. [91] and the gray solid line is a fit to the data. The measured G peaks are shown by the horizontal lines. The mean value of the impurity concentration from all the measured G peaks is $\bar{n} = (4.2 \pm 0.3) \times 10^{12} \text{ cm}^{-2}$, where the random and systematic errors were summed to obtain the maximum possible error. Na is expected to be the dominant impurity type based on the transfer process used [86]. Figure 4 presents a spatial distribution of the impurity concentration from Fig. 3 measured over the area $0.6 \times 0.8 \text{ cm}^2$ of the sample. In accordance with Fig. 3, the light gray, gray, and dark gray areas in the field of Fig. 4 correspond to the impurity concentrations varying from 3×10^{12} to $4 \times 10^{12} \text{ cm}^{-2}$, 4×10^{12} to $5 \times 10^{12} \text{ cm}^{-2}$, and from 5×10^{12} to $6 \times 10^{12} \text{ cm}^{-2}$, respectively.

The respective value of the chemical potential of our graphene sample at zero temperature is given by [92]

$$\mu = \hbar v_F \sqrt{\pi \bar{n}} = 0.24 \pm 0.01 \text{ eV}, \quad (7)$$

where the Fermi velocity $v_F \approx c/300$. According to Ref. [93], due to the relatively large value of the chemical potential, as in Eq. (7), it is almost independent on temperature. Because of

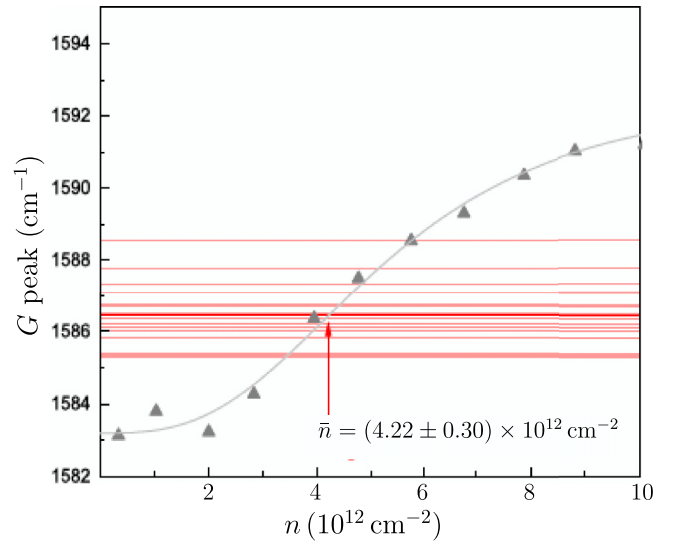


FIG. 3. The measured G -peak values from Raman spectroscopy compared to the charge concentration in graphene from Ref. [91]. The solid triangles are the values from Ref. [91] and the solid gray line is a best fit to the data. The G -peak values measured at equidistant points on the sample are shown by horizontal lines. The intersection identifies the impurity concentration. The average impurity concentration is shown by the arrow.

this, one can use the obtained value (7) both at zero and room temperatures.

We proceed now to measurements of the energy gap Δ . The energy gap of the graphene mounted on the fused silica was determined using scanning tunneling spectroscopy

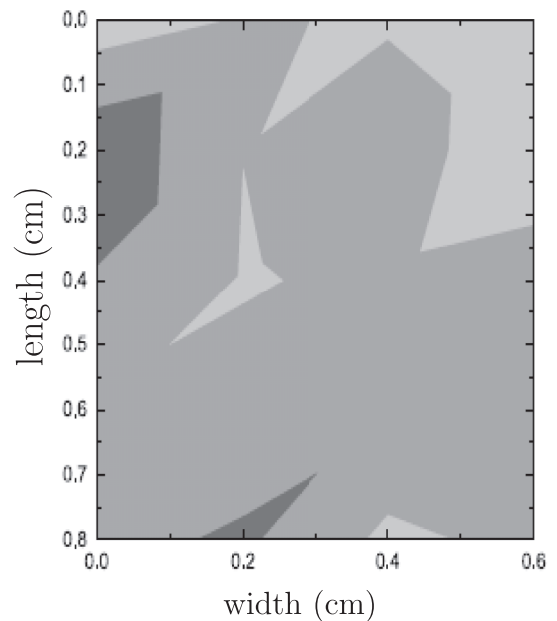


FIG. 4. The impurity concentration measured at different points over the $0.6 \times 0.8 \text{ cm}^2$ area of the sample from Fig. 3 is shown by the light gray, gray, and dark gray regions where it varies from 3×10^{12} to $4 \times 10^{12} \text{ cm}^{-2}$, 4×10^{12} to $5 \times 10^{12} \text{ cm}^{-2}$, and from 5×10^{12} to $6 \times 10^{12} \text{ cm}^{-2}$, respectively.

(STS) [94]. The STS measurements were performed using a Nanosurf Nano scanning tunneling microscope (STM). The probe was fabricated by mechanically cutting a Pt-Ir wire, generating a sharp tip. The graphene sample on the fused silica substrate was cut into $5 \times 5 \text{ mm}^2$ pieces and mounted onto metal puck holders using a conductive adhesive. Conduction between graphene surfaces and the metal puck was achieved by using the same conductive epoxy.

All experiments were performed in air at $22 \pm 1^\circ \text{C}$. The STM was kept in an enclosed environment on a floating optical table to minimize thermal and vibrational fluctuations. To select an appropriate region free from surface wrinkles and corrugations, rough microscopic scans ($50 \times 50 \text{ nm}^2$ to $10 \times 10 \text{ nm}^2$) of the surface topography were performed prior to spectroscopic measurements. The microscopic scans were performed with a bias voltage of 50 mV and a tunneling current of 1 nA.

The spectroscopic scans were performed in current-voltage mode where the measurement position and tip-sample separation distance were checked to be constant by monitoring the initial tunneling current prior to the spectroscopic scans. For the spectroscopic scans, the bias voltage was linearly ramped from -1.2 V to 1.2 V over a 100-ms period. As the experiments were carried out at room temperature, experiments at different periods of 10 ms and 50 ms were also tried and verified to lead to similar results. The final spectroscopic scans were all carried out with a 100-ms period and the tunneling currents were recorded at 256 equal time intervals during each ramp from -1.2 V to $+1.2 \text{ V}$. The experiment was repeated 3–4 times till a reproducible spectrogram was obtained. The entire experiment was repeated at 50 different positions on three different samples.

From the tunneling current I as a function of the bias voltage V_{bias} , the differential conductance, dI/dV_{bias} as a function of the bias voltage was determined. An averaged differential conductance as a function of V_{bias} from the 50 different measured spectra obtained from the three different samples is shown in Fig. 5. The average minimum value of the differential conductance measured is shown as a horizontal dashed line. A U-shaped parabolic dependence of the differential conductance with bias voltage was observed. The V-shape differential conductance with bias voltage reported for a pristine graphene at low temperature was not observed due to room-temperature measurement as well as the presence of an energy gap from the presence of impurities [95,96] and the mechanical strain from the substrate [97,98], both of which modify the local density of states.

Previous Raman spectroscopy mapping of charge impurities on the sample (see Fig. 4) shows that the impurity density varies with position leading to variations in the differential conductance at different positions. The substrate-induced roughness also leads to similar variations with position [97–99]. To determine the band edge at negative voltage bias, the differential conductance curve in that region was extrapolated to intersect with the line of minimum dI/dV_{bias} [100]. The extrapolation was done using a semilog plot of the differential conductance. Uncertainties in the extrapolation are recorded as uncertainties in the determination of the band edge. This was repeated for the differential conductance curve at the positive bias to identify the band edge in that

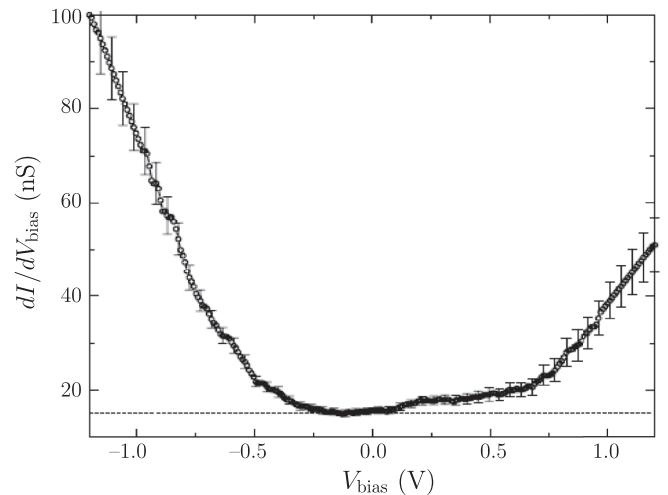


FIG. 5. The average differential conductance dI/dV_{bias} , measured from the scanning tunneling spectroscopy of the graphene sample as a function of the bias voltage. For clarity, the error bars are shown only at every fifth data point. The horizontal dashed line is the minimum average differential conductance measured.

region. The width of the energy gap was thus determined to be $\Delta = 0.29 \pm 0.05 \text{ eV}$ using this procedure.

The obtained values of the energy gap and chemical potentials are used in Secs. V and VI, where the gradients of the Casimir force are computed using the formalism of the polarization tensor.

IV. THEORY OF THERMAL CASIMIR INTERACTION FROM GRAPHENE USING THE POLARIZATION TENSOR IN THE EXPERIMENTAL CONFIGURATION

As mentioned in Sec. I, there are many theoretical approaches used in the literature for a description of the Casimir interaction in graphene systems. Here, we describe the gradient of the Casimir force in the experimental configuration by means of the Lifshitz theory which is valid for any planar layered structures with appropriately found reflection coefficients. In doing so, the response of Au and fused silica to the electromagnetic field is described by their frequency-dependent dielectric permittivities, whereas the response of graphene can be found precisely in the framework of the Dirac model using the polarization tensor in (2+1)-dimensional space-time. An employment of the Dirac model is fully justified because even at the shortest separation considered in our experiment ($a = 250 \text{ nm}$), the characteristic energy of the Casimir force $\hbar\omega_c = \hbar c/(2a) = 0.4 \text{ eV}$ is well within the application region of the Dirac model of graphene (according to recent results it is applicable up to 3 eV [101]). Because of this, one need not take into consideration the absorption peak of graphene at $\lambda = 270 \text{ nm}$ which corresponds to much higher energy $\hbar\omega = 2\pi\hbar c/\lambda \approx 4.59 \text{ eV}$.

Using the proximity force approximation (PFA) [35] (corresponding error in this experiment is very small and is taken into account below), the gradient of the Casimir force between an Au-coated sphere and a graphene-coated SiO_2 plate calculated at the laboratory temperature T takes the form

[74,77,82]

$$F'(a, T) = 2k_B T R \sum_{l=0}^{\infty} \int_0^{\infty} q_l k_{\perp} dk_{\perp} \times \sum_{\sigma} [r_{\sigma}^{-1}(i\xi_l, k_{\perp}) R_{\sigma}^{-1}(i\xi_l, k_{\perp}, T) e^{2aq_l} - 1]^{-1}. \quad (8)$$

In this equation, k_B is the Boltzmann constant, the prime on the first summation sign divides the term with $l = 0$ by 2, k_{\perp} is the magnitude of the wave vector projection on a graphene plane, the Matsubara frequencies are $\xi_l = 2\pi k_B T l / \hbar$, $q_l = \sqrt{k_{\perp}^2 + \xi_l^2 / c^2}$, and the summation in σ is over the two polarizations of the electromagnetic field, transverse magnetic ($\sigma = \text{TM}$) and transverse electric ($\sigma = \text{TE}$).

Now it is necessary to define the reflection coefficients r_{σ} and R_{σ} entering Eq. (8). In doing so, taking into account the sufficiently thick Au coating on the sphere and large thickness of the SiO₂ plate, the sphere can be considered as all-gold and the plate as a semispace [35]. Then, the coefficients r_{σ} on the boundary between Au and vacuum take the standard form [35–37]

$$r_{\text{TM}}(i\xi_l, k_{\perp}) = \frac{\varepsilon_l^{(1)} q_l - k_l^{(1)}}{\varepsilon_l^{(1)} q_l + k_l^{(1)}}, \quad r_{\text{TE}}(i\xi_l, k_{\perp}) = \frac{q_l - k_l^{(1)}}{q_l + k_l^{(1)}}, \quad (9)$$

where

$$k_l^{(n)} = k_l^{(n)}(k_{\perp}) = \sqrt{k_{\perp}^2 + \varepsilon_l^{(n)} \frac{\xi_l^2}{c^2}} \quad (10)$$

and $\varepsilon_l^{(n)} = \varepsilon^{(n)}(i\xi_l)$ are the dielectric permittivities of Au ($n = 1$) and SiO₂ ($n = 2$) calculated at the pure imaginary Matsubara frequencies.

The reflection coefficients R_{σ} on the boundary between the vacuum and graphene-coated plate are more involved because the plate material is described by the dielectric permittivity $\varepsilon_l^{(2)}$ whereas graphene — by the polarization tensor in (2+1)-dimensional space-time

$$\Pi_{\beta\gamma,l} \equiv \Pi_{\beta\gamma}(i\xi_l, k_{\perp}, T, \Delta, \mu), \quad (11)$$

where $\beta, \gamma = 0, 1, 2$. This tensor depends on temperature T and on the energy gap Δ and chemical potential μ of a graphene sheet. In fact, it has only two independent components [64–66]. It is most convenient to express the reflection coefficients via $\Pi_{00,l}$ and the following combination of the components Π_l defined as

$$\Pi_l = k_{\perp}^2 \Pi_{\beta,l}^{\beta} - q_l^2 \Pi_{00,l}, \quad (12)$$

where $\Pi_{\beta,l}^{\beta}$ (the summation in β is implied) is the trace of the polarization tensor.

Using the above notations, the reflection coefficients R_{σ} are given by [77,79,82]

$$R_{\text{TM}}(i\xi_l, k_{\perp}, T) = \frac{\hbar k_{\perp}^2 [\varepsilon_l^{(2)} q_l - k_l^{(2)}] + q_l k_l^{(2)} \Pi_{00,l}}{\hbar k_{\perp}^2 [\varepsilon_l^{(2)} q_l + k_l^{(2)}] + q_l k_l^{(2)} \Pi_{00,l}}, \quad (13)$$

$$R_{\text{TE}}(i\xi_l, k_{\perp}, T) = \frac{\hbar k_{\perp}^2 [q_l - k_l^{(2)}] - \Pi_l}{\hbar k_{\perp}^2 [q_l + k_l^{(2)}] + \Pi_l}.$$

To calculate the gradient of the Casimir force using Eqs. (8)–(13) one needs to have the values of the dielectric permittivities $\varepsilon_l^{(n)}$ and of the quantities $\Pi_{00,l}$ and Π_l as input information. As mentioned in Sec. I, the quantities $\varepsilon_l^{(n)}$ are obtained from the measured optical data for the complex index of refraction [41]. In the case of one test body coated with a graphene sheet, the reflection coefficient $R_{\text{TE}}(0, k_{\perp}, T)$ turns out to be very small. Because of this, the gradients of the Casimir force calculated by Eqs. (8)–(13) are almost independent of the type of extrapolation of the optical data to zero frequency discussed in Sec. I. Therefore, one can safely employ the values of $\varepsilon_l^{(n)}$ available in the literature [35–37] obtained using any extrapolation (i.e., taking into account or disregarding the relaxation properties of conduction electrons), leading to coinciding results. This gives the possibility to consider the reflection coefficients r_{σ} as independent of T .

The quantities $\Pi_{00,l}$ and Π_l are conveniently presented as the sums of two contributions:

$$\Pi_{00,l} = \Pi_{00,l}^{(0)} + \Pi_{00,l}^{(1)}, \quad \Pi_l = \Pi_l^{(0)} + \Pi_l^{(1)}. \quad (14)$$

The first terms on the right-hand sides of these equations are related to the polarization tensor of an undoped graphene with $\mu = 0$, arbitrary value of the energy gap Δ , at zero temperature $T = 0$, but calculated at the pure imaginary Matsubara frequencies $\omega = i\xi_l$. This means that the quantities $\Pi_{00,l}^{(0)}$ and $\Pi_l^{(0)}$ take into account only an implicit dependence of the polarization tensor on temperature through the Matsubara frequencies. The second terms on the right-hand sides of Eq. (14) result from an explicit dependence of the polarization tensor on temperature T and on the chemical potential μ . In so doing, they also depend on Δ .

The explicit expressions for $\Pi_{00,l}^{(0)}$ and $\Pi_l^{(0)}$ are given by [63,64]

$$\Pi_{00,l}^{(0)} = \frac{\alpha \hbar k_{\perp}^2}{\tilde{q}_l} \Psi(D_l), \quad \Pi_l^{(0)} = \alpha \hbar \tilde{q}_l \Psi(D_l), \quad (15)$$

where $\alpha = e^2 / (\hbar c)$ is the fine structure constant and

$$\tilde{q}_l = \left(\frac{v_F^2}{c^2} k_{\perp}^2 + \frac{\xi_l^2}{c^2} \right)^{1/2}, \quad D_l = \frac{\Delta}{\hbar c \tilde{q}_l},$$

$$\Psi(x) = 2 \left[x + (1 - x^2) \arctan \frac{1}{x} \right]. \quad (16)$$

The exact expressions for $\Pi_{00,l}^{(1)}$ and $\Pi_l^{(1)}$ are more involved. They can be conveniently presented in the form [66,79]

$$\Pi_{00,l}^{(1)} = \frac{4\alpha \hbar c^2 \tilde{q}_l}{v_F^2} \int_{D_l}^{\infty} du \left(\sum_{\kappa=\pm 1} \frac{1}{e^{B_l u + \kappa \frac{\mu}{k_B T}} + 1} \right) \times \left[1 - \text{Re} \frac{1 - u^2 + 2i\gamma_l u}{(1 - u^2 + 2i\gamma_l u + D_l^2 - \gamma_l^2 D_l^2)^{1/2}} \right],$$

$$\Pi_l^{(1)} = -\frac{4\alpha \hbar \tilde{q}_l \xi_l^2}{v_F^2} \int_{D_l}^{\infty} du \left(\sum_{\kappa=\pm 1} \frac{1}{e^{B_l u + \kappa \frac{\mu}{k_B T}} + 1} \right) \times \left[1 - \text{Re} \frac{(1 + i\gamma_l^{-1} u)^2 + (\gamma_l^{-2} - 1) D_l^2}{(1 - u^2 + 2i\gamma_l u + D_l^2 - \gamma_l^2 D_l^2)^{1/2}} \right], \quad (17)$$

where $\gamma_l \equiv \xi_l/(c\tilde{q}_l)$ and $B_l \equiv \hbar c\tilde{q}_l/(2k_B T)$.

To gain better insight into the meaning of two contributions in Eq. (14), we note that the quantity (17) can be also presented as

$$\begin{aligned}\Pi_{00,l}^{(1)} &= A_{00,l}(\Delta, \mu) + B_{00,l}(T, \Delta, \mu), \\ \Pi_l^{(1)} &= A_l(\Delta, \mu) + B_l(T, \Delta, \mu),\end{aligned}\quad (18)$$

$$\begin{aligned}\Pi_{00,0} &= \alpha\hbar c \frac{k_{\perp}}{v_F} \Psi(D_0) + \frac{8\alpha k_B T c}{v_F^2} \sum_{\kappa=\pm 1} \ln(e^{\kappa \frac{\mu}{k_B T}} + e^{-\frac{\Delta}{2k_B T}}) - \frac{4\alpha\hbar c k_{\perp}}{v_F} \int_{D_0}^{\sqrt{1+D_0^2}} du \left(\sum_{\kappa=\pm 1} \frac{1}{e^{B_0 u + \kappa \frac{\mu}{k_B T}} + 1} \right) \frac{1-u^2}{\sqrt{1-u^2+D_0^2}}, \\ \Pi_0 &= \alpha\hbar \frac{v_F k_{\perp}^3}{c} \Psi(D_0) + 4\alpha\hbar \frac{v_F k_{\perp}^3}{c} \int_{D_0}^{\sqrt{1+D_0^2}} du \left(\sum_{\kappa=\pm 1} \frac{1}{e^{B_0 u + \kappa \frac{\mu}{k_B T}} + 1} \right) \frac{-u^2 + D_0^2}{\sqrt{1-u^2+D_0^2}},\end{aligned}\quad (19)$$

where, according to the above notations, $D_0 = \Delta/(\hbar v_F k_{\perp})$ and $B_0 = \hbar v_F k_{\perp}/(2k_B T)$.

At room temperature and $a > 100$ nm one can obtain also much simpler approximate expressions for $\Pi_{00,l}$ and Π_l with $l \geq 1$ than the exact ones given by Eqs. (14), (15), and (17). For this purpose, the condition $\xi_1 \gg v_F/(2a)$ should be used leading to [77,79]

$$\begin{aligned}\Pi_{00,l} &\approx \alpha\hbar c \frac{k_{\perp}^2}{\xi_l} \left[\Psi\left(\frac{\Delta}{\hbar\xi_l}\right) + Y_l(T, \Delta, \mu) \right], \\ \Pi_l &\approx \alpha\hbar\xi_l \frac{k_{\perp}^2}{c} \left[\Psi\left(\frac{\Delta}{\hbar\xi_l}\right) + Y_l(T, \Delta, \mu) \right],\end{aligned}\quad (20)$$

where

$$\begin{aligned}Y_l(T, \Delta, \mu) &= 2 \int_{\Delta/(\hbar\xi_l)}^{\infty} du \left(\sum_{\kappa=\pm 1} \frac{1}{e^{B_l u + \kappa \frac{\mu}{k_B T}} + 1} \right) \\ &\quad \times \frac{u^2 + \left(\frac{\Delta}{\hbar\xi_l}\right)^2}{u^2 + 1}.\end{aligned}\quad (21)$$

It was shown [77,79] that numerical computations of the Casimir force using the exact expressions (14), (15), and (17) for the polarization tensor and, alternatively, the exact expressions (19) for $l = 0$ but the approximate expressions (20) for $l \geq 1$ at room temperature and $a \geq 100$ nm lead to computational results differing by less than 0.01%.

Below we consider not only the gradient of the Casimir force between an Au-coated sphere and graphene-coated substrate but also the thermal correction to it defined as

$$\Delta_T F'(a, T) = F'(a, T) - F'(a, 0).\quad (22)$$

The gradient of the Casimir force at zero temperature, $F'(a, 0)$, can be calculated by the Lifshitz formula (8) where a summation over the discrete Matsubara frequencies should be replaced with an integration over the axis of pure imaginary frequency according to

$$k_B T \sum_{l=0}^{\infty} \rightarrow \frac{\hbar}{2\pi} \int_0^{\infty} d\xi.\quad (23)$$

This means that in Eq. (8) one should replace ξ_l and q_l with ξ and q . The respective replacements, which also include the

where $A_{00,l}$ and A_l do not depend on T and go to zero with vanishing μ whereas $B_{00,l}$ and B_l go to zero with vanishing T .

In practical computations, it is convenient to consider separately the contributions to Eq. (8) with $l = 0$ and with all $l \geq 1$. Thus, from Eqs. (14), (15), and (17) for $l = 0$ one obtains

changes of $k_l^{(n)}$ for $k^{(n)}$, \tilde{q}_l for \tilde{q} , $\Pi_{00,l}$ for Π_{00} , and Π_l for Π , should be made in Eqs. (9)–(17).

To calculate the gradients of the Casimir force at zero temperature, one also needs explicit expressions for the quantities

$$\begin{aligned}\Pi_{00} &\equiv \Pi_{00}(i\xi, k_{\perp}, 0, \Delta, \mu), \\ \Pi &\equiv \Pi(i\xi, k_{\perp}, 0, \Delta, \mu).\end{aligned}\quad (24)$$

They can be obtained using Eqs. (14), (15), and (17) by performing integration with respect to u . The obtained results in the cases $2\mu > \Delta$ and $2\mu \leq \Delta$ are different. For the graphene sample used in our experiment the condition $2\mu > \Delta$ is satisfied (see Sec. III) and after calculation one arrives at [79]

$$\begin{aligned}\Pi_{00} &= \frac{8\alpha c \mu}{v_F^2} - \frac{\alpha\hbar k_{\perp}^2}{\tilde{q}} \{ 2M \text{Im}(y_{\Delta,\mu} \sqrt{1+y_{\Delta,\mu}^2}) \\ &\quad + (2-M)[2\text{Im} \ln(y_{\Delta,\mu} + \sqrt{1+y_{\Delta,\mu}^2}) - \pi] \}, \\ \Pi &= -\frac{8\alpha\xi^2 \mu}{c v_F^2} + 2\alpha\hbar\tilde{q}k_{\perp}^2 \left[M \text{Im}(y_{\Delta,\mu} \sqrt{1+y_{\Delta,\mu}^2}) \right. \\ &\quad \left. - (2-M) \text{Im} \ln(y_{\Delta,\mu} + \sqrt{1+y_{\Delta,\mu}^2}) + \frac{\pi}{2}(2-M) \right].\end{aligned}\quad (25)$$

Here, the following notations are introduced:

$$M = 1 + D^2, \quad y_{\Delta,\mu} = \frac{\hbar\xi + 2i\mu}{\hbar v_F k_{\perp} \sqrt{M}}.\quad (26)$$

In the opposite case, $2\mu \leq \Delta$, one has [79]

$$\Pi_{00} = \Pi_{00}^{(0)}, \quad \Pi = \Pi^{(0)},\quad (27)$$

where $\Pi_{00}^{(0)}$ and $\Pi^{(0)}$ are defined in Eq. (15) with a replacement of ξ_l for ξ .

We postpone a comparison between theoretical predictions of the above theory and the measurement data to Sec. VI. In the next section, we consider the relative magnitudes of the thermal correction and its constituents in the total Casimir interaction for both real and pristine graphene samples and provide a qualitative discussion of the origin and physical nature of the unusually big thermal effect arising in graphene systems at short separations.

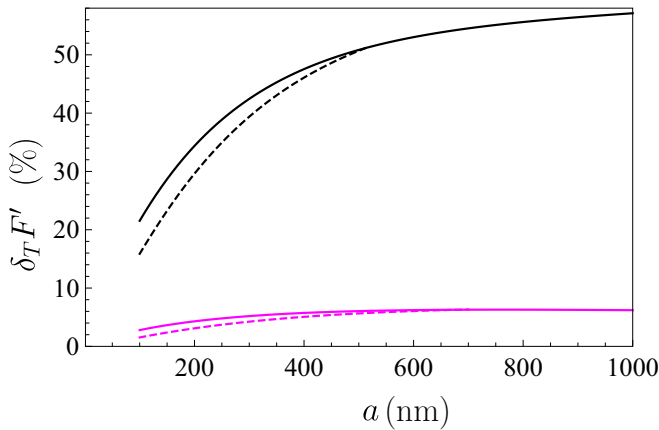


FIG. 6. The computational results for the relative thermal correction to the gradient of the Casimir force are shown as functions of separation by the bottom and top pairs of lines for an Au-coated sphere interacting either with real graphene sheet deposited on a SiO₂ plate or with freestanding real graphene sheet in vacuum, respectively. The solid and dashed lines in each pair are computed including and neglecting the explicit dependence of the polarization tensor on temperature as a parameter, respectively.

V. PHYSICAL NATURE AND MAGNITUDE OF THE THERMAL EFFECT IN REAL AND PRISTINE GRAPHENE SAMPLES

Let us calculate the relative thermal correction to the gradient of the Casimir force acting between an Au-coated sphere of radius $R = 60.35 \mu\text{m}$ and a graphene-coated SiO₂ plate which is given by

$$\delta_T F'(a, T) = \frac{\Delta_T F'(a, T)}{F'(a, 0)}, \quad (28)$$

where the absolute thermal correction $\Delta_T F'$ is defined in Eq. (22). We consider the graphene sheet with the experimental parameters $\mu = 0.24 \text{ eV}$ and $\Delta = 0.29 \text{ eV}$. Computations of the quantity $F'(a, T)$ are performed by Eqs. (8), (9), (13), (19), and (20) and of the quantity $F'(a, 0)$ — by Eqs. (8), (9), (13), (23), and (25).

The computational results for $\delta_T F'$ at $T = 294 \text{ K}$ as a function of separation are presented by the bottom solid line in Fig. 6. As seen in Fig. 6, at separations of $a = 100, 200, 300,$ and 400 nm , the relative thermal correction in the experimental configuration reaches 2.79%, 4.29%, 5.19%, and 5.73% of the force gradient at $T = 0$, respectively. This effect is similar in magnitude to that predicted by the Lifshitz theory for the Casimir interaction between metallic test bodies described with inclusion of the dissipation of conduction electrons. As discussed in Sec. I, for metals this prediction was excluded by the results of many experiments.

The bottom dashed line in Fig. 6 shows the computational results for $\delta_T F'$ under a condition that the quantity $F'(a, T)$ is computed using the polarization tensor taken at $T = 0$. This means that the thermal correction in this case is implicit, i.e., fully determined by a summation over the Matsubara frequencies, whereas an explicit dependence of the polarization tensor on temperature as a parameter is disregarded. As seen from the bottom dashed line in Fig. 6, at separations of $a = 100,$

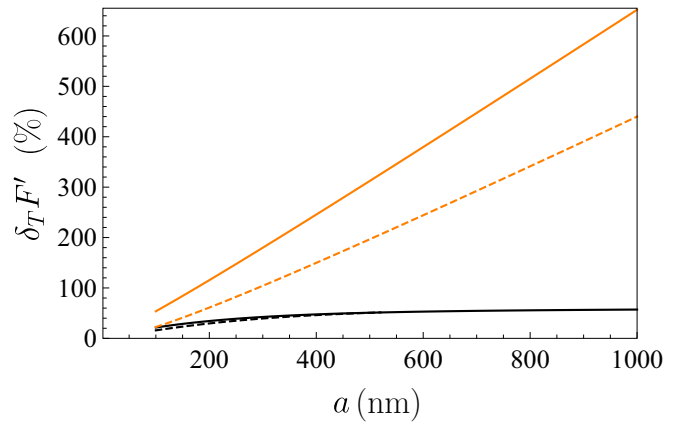


FIG. 7. The computational results for the relative thermal correction to the gradient of the Casimir force are shown as functions of separation by the bottom and top pairs of lines for an Au-coated sphere interacting with the freestanding either real or pristine graphene sheet in vacuum, respectively. The solid and dashed lines in each pair are computed including and neglecting the explicit dependence of the polarization tensor on temperature as a parameter, respectively.

200, 300, and 400 nm, the implicit thermal correction is equal to 1.53%, 3.10%, 4.24%, and 5.06%, respectively. Thus, with increasing separation, the role of explicit dependence of the polarization tensor on temperature gradually decreases and becomes negligibly small at $a \geq 700 \text{ nm}$.

To determine the role of a SiO₂ substrate in the above results, we repeat computations of the relative thermal correction $\delta_T F'$ for the configuration of an Au sphere and a freestanding graphene sheet preserving unchanged all other parameters of the experimental configuration. The computational results are shown by the top pair of solid and dashed lines having the same meaning as the respective lines of the bottom pair. As seen from the top solid line in Fig. 6, at separations of $a = 100, 200, 300,$ and 400 nm , the thermal correction (28) reaches much larger values of 21.5%, 34.4%, 42.4%, and 47.5%, respectively. This means that in the absence of a substrate, the thermal effect inherent to the graphene sheet manifests itself more vividly. The top dashed line in Fig. 6 illustrates the contribution of an implicit thermal effect due to a summation over the Matsubara frequencies to the total thermal correction in the case of a freestanding graphene sheet interacting with an Au-coated sphere. As seen in Fig. 6, at separations of $a = 100, 200, 300,$ and 400 nm , the implicit thermal effect contributes 15.9%, 29.6%, 39.4%, and 46.1% of the force gradient at $T = 0$. At separations exceeding 500 nm, an explicit dependence of the polarization tensor on T does not lead to a noticeable contribution to the thermal correction (28).

Up to this point, we have considered the graphene sample with nonzero Δ and μ used in our experiment. It should be noted that for a pristine graphene possessing $\Delta = \mu = 0$, the thermal effect in the Casimir interaction at short separation distances would be even much larger. To illustrate this, in Fig. 7 the computational results for $\delta_T F'$ in the configuration of an Au-coated sphere interacting with a freestanding pristine graphene sheet are shown by the top pair of solid

TABLE I. Separation distances in μm where the zero-frequency term of the Lifshitz formula for the case of two parallel plates made of materials indicated in column 1 contributes more than 90% (column 2), 95% (column 3), and 99% (column 4) of the total Casimir pressure at larger separations.

Plate materials	a (μm)		
	90% of P	95% of P	99% of P
SiO ₂ —Au	3.6	4.2	5.5
(SiO ₂ +real graphene)—Au	3.1	3.7	5.0
(real graphene)—Au	0.8	1.3	2.7
(pristine graphene)—Au	0.7	1.15	2.5
(pristine graphene)—(pristine graphene)	0.11	0.17	0.38

and dashed lines as functions of separation (the total and implicit thermal corrections, respectively). As seen in Fig. 7, at separations of $a = 100, 200, 300, 400, 700,$ and 1000 nm, the thermal correction $\delta_T F'$ defined in Eq. (28) is equal to 53.7%, 115.5%, 179.8%, 245.6%, 447.1%, and 659.9%, respectively. According to Fig. 7, for pristine graphene the implicit thermal correction plays a smaller role than for the experimental graphene sample. Thus, at $a = 100, 200, 300, 400, 700,$ and 1000 nm, it is equal to 22.5%, 61.1%, 104.3%, 149.8%, 292.5%, and 439.9%, respectively. As a result, the explicit thermal dependence of the polarization tensor contributes 31.2%, 54.4%, 75.5%, 95.8%, 154.6%, and 212.0% of $F'(a, 0)$ at the same respective separations and does not disappear when the separation increases.

For comparison purposes, the bottom pair of solid and dashed lines in Fig. 7 reproduces the top pair of lines in Fig. 6 related to the case of an Au-coated sphere interacting with a freestanding real graphene sheet used in our experiment (with $\Delta = 0.29$ eV and $\mu = 0.24$ eV). From Fig. 7, it is seen that the replacement of a real with a pristine graphene sheet leads to a qualitatively large increase of the thermal correction to the gradient of the Casimir force at short separations.

From the above results, it is seen that even the presence of a graphene sheet deposited on a substrate significantly increases the thermal effect in the Casimir interaction at short separations which constitutes only a small fraction of percent for both metallic and dielectric materials. Because of this, it is interesting to consider the so-called thermal regime of the Casimir interaction in the presence of graphene which takes place under the condition

$$F'(a, 0) \ll \Delta_T F'(a, T), \quad (29)$$

i.e., when the thermal correction (22) determines the major part of the force gradient at temperature T . This is the case when the term of the Lifshitz formula (8) with $l = 0$ becomes much larger than the sum of all remaining terms with $l \geq 1$.

To determine the role of graphene in reaching the thermal regime of the Casimir interaction, we have computed separation distances between the parallel plates made of different materials such that at larger separations the Casimir pressure given by the zero-frequency term of the Lifshitz formula contributes more than 90%, 95%, and 99% of the total Casimir pressure. The following cases were considered: an Au plate and a SiO₂ plate; an Au plate and a SiO₂ plate coated with real graphene sheet used in our experiment; an

Au plate and a real graphene sheet; an Au plate and a pristine graphene sheet; two pristine graphene sheets. The obtained computational results are presented in Table I [we recall that according to PFA the Casimir pressure between two parallel plates $P = -F'/(2\pi R)$, i.e., is proportional to the gradient of the Casimir force in sphere-plate geometry used in our experiment].

As seen in Table I, the presence of a graphene sheet significantly decreases the minimum separation distance from which the Casimir interaction is going into the thermal regime. The thermal regime starts at especially short separations in the absence of a material substrate and for the pristine graphene sheets. Thus, for SiO₂—Au plates, the full thermal regime (99% of the Casimir pressure) is reached only at $a \geq 5.5 \mu\text{m}$, whereas for two pristine graphene sheets it is achieved at $a \geq 0.38 \mu\text{m}$.

In the end of this section, we present a qualitative discussion of the physical reasons why for two pristine graphene sheets the thermal regime starts at such short separations. It is common knowledge that for ordinary materials the thermal regime starts at separations a satisfying the condition [35]

$$\frac{1}{2a} \ll \frac{\xi_1}{c} = 2\pi \frac{k_B T}{\hbar c}. \quad (30)$$

This condition can be rewritten as

$$k_B T \gg \frac{1}{2\pi} k_B T_{\text{eff}}, \quad k_B T_{\text{eff}} \equiv \frac{\hbar c}{2a}, \quad (31)$$

where T_{eff} is the so-called effective temperature. Thus, according to numerical computations in Table I, for two plates made of Au and SiO₂, the full thermal regime is reached at $a = 5.5 \mu\text{m}$, which corresponds to the effective temperature $T_{\text{eff}} \approx 208.3$ K. In doing so, $T_{\text{eff}}/(2\pi) \approx 33.2$ K so that at room temperature the inequality (31) is well satisfied. Because of this, the thermal regime is also called the high-temperature limit. In the high-temperature limit, the Casimir pressure determined by all Matsubara frequencies with $l \geq 1$ is of the order of [35]

$$P_{l \geq 1}(a, T) \sim \exp\left(-2\pi \frac{T}{T_{\text{eff}}}\right), \quad (32)$$

i.e., is exponentially small.

For graphene, however, the situation is more complicated because the reflection coefficients do not have the standard Fresnel form (9) but depend on the polarization tensor. The major contribution to the Casimir pressure between two

graphene sheets is given by the TM polarization. From Eq. (8), we have

$$P_{\text{gr}}(a, T) \approx -\frac{k_B T}{\pi} \sum_{l=0}^{\infty} \int_0^{\infty} q_l k_{\perp} dk_{\perp} \frac{r_{\text{TM,gr}}^2(i\xi_l, k_{\perp}) e^{-2aq_l}}{1 - r_{\text{TM,gr}}^2(i\xi_l, k_{\perp}) e^{-2aq_l}}, \quad (33)$$

where the reflection coefficient on a freestanding graphene sheet $r_{\text{TM,gr}}$ is obtained from R_{TM} defined in Eq. (13) by putting the dielectric permittivity of a substrate $\epsilon_l^{(2)}$ equal to unity:

$$r_{\text{TM,gr}}(i\xi_l, k_{\perp}) = \frac{q_l \Pi_{00,l}}{2\hbar k_{\perp}^2 + q_l \Pi_{00,l}}. \quad (34)$$

To understand the qualitative physical reasons why graphene already has a large thermal effect at relatively short separations, we restrict ourselves to the polarization tensor taken at $T = 0$ but calculated at the imaginary Matsubara frequencies (an account of the explicit temperature dependence may only increase the thermal effect). Then, from Eqs. (15) and (27), one finds

$$\Pi_{00,l} = \frac{\pi \alpha \hbar k_{\perp}^2}{\tilde{q}_l}, \quad (35)$$

where we have taken into account that for a pristine graphene in accordance with Eq. (16), it holds $\Psi(0) = \pi$.

Substituting Eq. (35) in Eq. (34), we obtain

$$r_{\text{TM,gr}}(i\xi_l, k_{\perp}) = \frac{\pi \alpha q_l}{\pi \alpha q_l + 2\tilde{q}_l}, \quad (36)$$

where q_l is defined below Eq. (8) and \tilde{q}_l in Eq. (16).

In the term of the Lifshitz formula (33) with $l = 0$, the reflection coefficient (36) takes the value

$$r_{\text{TM,gr}}(0, k_{\perp}) = \frac{\pi \alpha}{\pi \alpha + 2\frac{v_F}{c}} \approx 0.775. \quad (37)$$

The distinctive feature of graphene is that the reflection coefficient (36) depends on both c and v_F . Because of this, one can consider the region of separations where

$$\frac{v_F}{2a} \ll \xi_1 \ll \frac{c}{2a}. \quad (38)$$

The latter of these two inequalities is just the opposite to the condition (30) required for reaching the thermal regime between ordinary materials. However, under the inequalities (38), the reflection coefficient (36) with $l = 1$ can be approximately presented in the form

$$r_{\text{TM,gr}}(i\xi_1, k_{\perp}) = \frac{\pi \alpha}{2a\left(\frac{\pi \alpha}{2a} + 2\frac{\xi_1}{c}\right)} = \frac{\pi \alpha}{\pi \alpha + \frac{4a\xi_1}{c}}. \quad (39)$$

Here, we used that the major contribution to Eq. (33) is given by $k_{\perp} \approx 1/(2a)$ and that Eq. (38) results in $q_1 \approx 1/(2a)$ and $\tilde{q}_1 \approx \xi_1/c$. Taking into account that according to Eq. (38) $v_F \ll 2a\xi_1$, one concludes from Eqs. (37) and (39) that

$$r_{\text{TM,gr}}(i\xi_1, k_{\perp}) < r_{\text{TM,gr}}(0, k_{\perp}). \quad (40)$$

The left-hand side of this inequality further decreases if ξ_1 is replaced for ξ_l with $l > 1$. Thus, under the condition (38), a contribution of the zero-frequency term to Eq. (33) may become dominant in accordance to the results of numerical computations.

The first inequality in Eq. (38) can be identically rewritten in the form

$$k_B T \gg \frac{1}{2\pi} k_B T_{\text{eff}}^{\text{gr}}, \quad k_B T_{\text{eff}}^{\text{gr}} \equiv \frac{\hbar v_F}{2a}, \quad (41)$$

which is similar to Eq. (31). Thus, for graphene, in addition to the standard effective temperature T_{eff} defined in Eq. (31), there exists one more effective temperature $T_{\text{eff}}^{\text{gr}}$ defined in Eq. (41) which is lower than T_{eff} by a factor of 300. According to Ref. [45], the big thermal effect in the Casimir interaction between two graphene sheets at short separations is controlled by the effective temperature $T_{\text{eff}}^{\text{gr}}$. Our computational results and above qualitative estimations show that the thermal regime of the Casimir interaction in graphene systems is governed by two effective temperatures $T_{\text{eff}}^{\text{gr}}$ and T_{eff} . In doing so, at short separations, the thermal regime is determined by the much lower temperature $T_{\text{eff}}^{\text{gr}}$.

VI. COMPARISON BETWEEN EXPERIMENT AND THEORY

The gradients of the Casimir force $F'(a, T)$ between an Au-coated sphere of $R = 60.35 \pm 0.05 \mu\text{m}$ radius and a graphene-coated SiO_2 substrate at $T = 294.0 \pm 0.5 \text{ K}$ temperature were computed by Eqs. (8), (9), (13), (19), and (20) using the experimental values of the energy gap $\Delta = 2.9 \pm 0.05 \text{ eV}$ and chemical potential $\mu = 0.24 \pm 0.01 \text{ eV}$ (see Sec. III).

It is well known that the Casimir interaction is influenced by roughness on the interacting surfaces [35,36,102–104]. In the case of small stochastic roughness with the rms amplitudes $\delta_s = 0.9 \pm 0.1 \text{ nm}$ and $\delta_g = 1.5 \pm 0.1 \text{ nm}$ on the sphere and graphene surfaces, respectively (see Sec. II), it can be taken into account multiplicatively [35,36] resulting in the final expression for the gradient of theoretical Casimir force:

$$F'_{\text{theor}}(a, T) = \left(1 + 10 \frac{\delta_s^2 + \delta_g^2}{a^2}\right) F'(a, T). \quad (42)$$

This expression was used to compute the upper and lower boundaries of the top theoretical bands in Fig. 2 presenting allowed values of the Casimir force gradient at $T = 294 \text{ K}$. These boundaries were computed in the following most conservative way, taking a proper account of all errors which are present in the parameters used.

Thus, the upper boundary lines of the theoretical bands were calculated with the largest allowed value of the chemical potential $\mu = 0.25 \text{ eV}$ and the smallest allowed value of the energy gap $\Delta = 0.24 \text{ eV}$. This is explained by the fact that an increase of μ with fixed Δ leads to a larger F' whereas an increase of Δ at a constant μ results in a smaller F' [79]. The obtained theoretical bands for F'_{theor} were widened to take into account the errors in the sphere radius and the 0.5% error in the force gradients arising from uncertainties in the optical data of Au and SiO_2 (an error in the laboratory temperature indicated above does not influence on the obtained results).

The theoretical bands for F'_{theor} were also widened to take into account small errors of PFA used in Eq. (8). As was shown in the literature [105–109], when using the PFA, one obtains slightly increased force gradients as compared to the exact computational results in the sphere-plate geometry.

Because of this, we did not correct the upper lines of the theoretical bands for the PFA error but introduced the maximum possible correction factor of $(1 - a/R)$ to the lower boundary lines.

As seen in Fig. 2, the upper theoretical bands computed at $T = 294$ K are in a very good agreement with the measured gradients of the Casimir force indicated as crosses over the entire measurement range from 250 to 700 nm. The question arises as to whether the measurement data demonstrate the presence of an unusually big thermal effect in the Casimir force from graphene at short separations which is considered in Sec. V.

To answer this question, we have computed the gradients of the Casimir force, $F'(a, 0)$, at zero temperature by using Eqs. (8), (9), (13), (23), and (25) for the same parameters of the experimental configuration indicated above. The obtained values of $F'(a, 0)$ were substituted to Eq. (42) and the values of $F'_{\text{theor}}(a, 0)$ were calculated. The latter were used to find the upper and lower boundaries of the theoretical bands for the Casimir force gradient at $T = 0$ in the same conservative way as described above in the case of $T = 294$ K. The results of this calculation are presented by the bottom bands in Fig. 2. As seen in Fig. 2, the bottom theoretical bands computed at $T = 0$ are more narrow than the top ones computed at $T = 294$ K. This is because our graphene sample possesses a relatively large value of $\mu = 0.24$ eV. Calculations show that for such large values of the chemical potential an impact of the energy gap on the polarization tensor (and, as a consequence, on the reflection coefficients and force gradients) at $T = 0$ is considerably suppressed, as compared to the case of $T = 294$ K.

From Fig. 2 it is seen that the measurement data exclude the theoretical predictions at $T = 0$ shown by the bottom bands over the wide separation region from 250 to 517 nm and, thus, demonstrate the thermal effect in the Casimir interaction arising from our graphene sample.

For a more illustrative demonstration of the observed thermal effect, we also employ another way of comparison between experiment and theory based on a consideration of differences between the theoretical and mean experimental force gradients [23,25,33,35,36],

$$F'_{\text{theor}}(a_i, \tilde{T}) - F'_{\text{expt}}(a_i, T), \quad (43)$$

where the experimental force gradients are given by the centers of the crosses in Fig. 2 and the theoretical ones are computed with a step of 1 nm as described above.

In Fig. 8, we plot the quantity (43) as a function of separation by the top and bottom sets of dots obtained at $\tilde{T} = T = 294$ K and $\tilde{T} = 0$ K, $T = 294$ K, respectively. The confidence bands for the quantity (43) found at $\tilde{T} = T = 294$ K (solid lines) and $\tilde{T} = 0$ K, $T = 294$ K (dashed lines), respectively, take into account both the theoretical and experimental errors determined at the 67% confidence level. Note that in addition to the theoretical errors considered previously, now we also take into account an error arising from the fact that the quantities $F'_{\text{theor}}(a_i, \tilde{T})$ in Eq. (43) are computed not over some separation region but at the experimental separations a_i determined with an error Δa_i . The bands shown by the solid and dashed lines are slightly different because, as discussed above, for our graphene sample an error in the energy gap

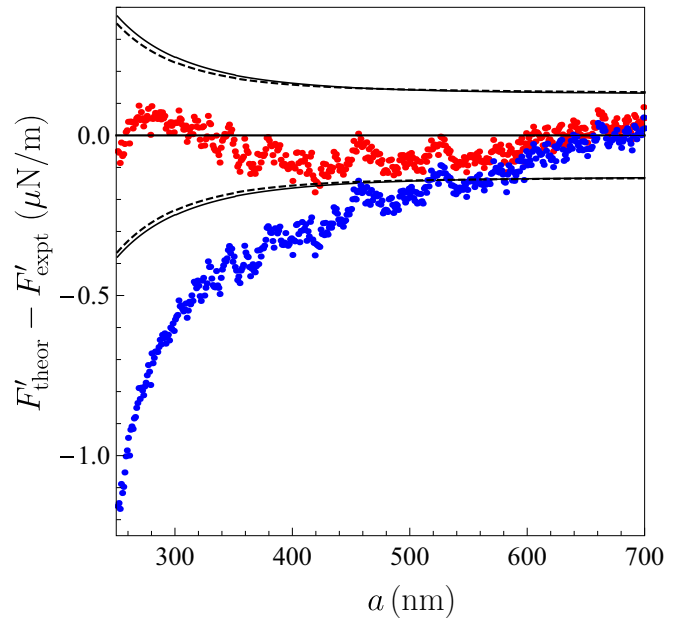


FIG. 8. The differences between theoretical gradients of the Casimir force computed either at $\tilde{T} = 294$ K (top set of dots) or at $\tilde{T} = 0$ K (bottom set of dots) and mean experimental gradients are shown as functions of separation. The solid and dashed lines indicate the borders of the confidence intervals for the top and bottom sets of dots, respectively, found at the 67% confidence level.

leads to different errors in the force gradients at $\tilde{T} = 0$ and at $\tilde{T} = 294$ K.

As seen in Fig. 8, within the entire range of separations from 250 to 700 nm the top set of dots found at $\tilde{T} = 294$ K is inside the confidence band shown by the solid lines. This means that the theoretical gradients of the Casimir force computed at $\tilde{T} = 294$ K are consistent with the measurement data. At the same time, the bottom set of dots found at $\tilde{T} = 0$ K is outside the confidence band shown by the dashed lines over the wide range of separations from 250 to 517 nm, i.e., the theoretical results computed at $\tilde{T} = 0$ are experimentally excluded. These conclusions are in agreement with those obtained above based on Fig. 2.

The differences between the measurement data at $T = 294$ K and computed at $T = 0$ force gradients can be used to plot the thermal correction $\Delta_T F'$ defined in Eq. (22). In Fig. 9, it is shown by dots as a function of separation in the region where the theory at $T = 0$ is experimentally excluded and cannot be used for interpretation of the measurement data. The values of $\Delta_T F'$ at different separations shown in Fig. 9 are consistent with the theoretical values of $\delta_T F'$ computed in Sec. V for our graphene sample. This can be easily verified by using the computational results for the gradients of the Casimir force presented in Fig. 2. Thus, the performed experiment demonstrates an unusual thermal effect in graphene systems which becomes noticeable even at relatively short separations of a few hundred nanometers.

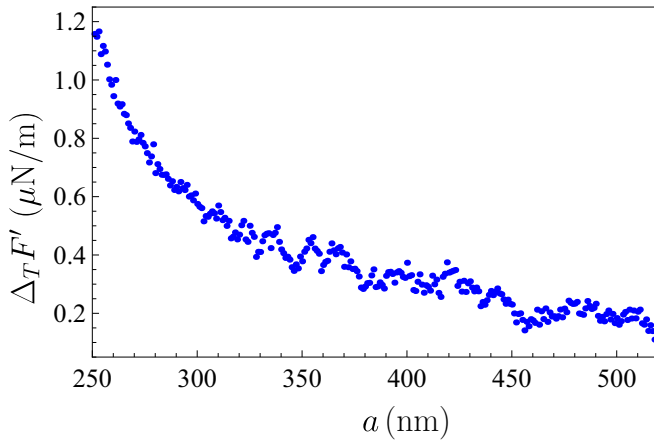


FIG. 9. The thermal correction to the gradient of the Casimir force found as a difference between the mean experimental gradients measured at $T = 294$ K and the theoretical ones computed at $T = 0$ K is shown by dots as a function of separation.

VII. CONCLUSIONS AND DISCUSSION

In the foregoing, we have described measurements of the thermal Casimir interaction between an Au-coated sphere and a graphene-coated substrate performed at $T = 294$ K in high vacuum by means of a custom-built AFM cantilever-based setup operated in the dynamic regime. Using the two sets of measurements each of which contains 21 experimental runs, we have obtained the mean gradients of the Casimir force and determined their random, systematic, and total experimental errors over the separation region between a sphere and a graphene sheet from 250 to 700 nm. In doing so, all the experimental parameters, including the absolute separations and their errors, were determined by means of electrostatic calibration. For the substrate supporting the graphene sheet, a sufficiently thick fused silica plate has been used which, as was proposed in Ref. [74], should make it possible to observe the unusual thermal effect in graphene systems at short separations predicted in Ref. [45].

According to the literature provided in Sec. I, an experimental discovery of this effect for graphene would be of great fundamental importance because a similar effect had long been predicted by the Lifshitz theory for metals described by the conventional Drude response function [43], but was experimentally excluded by numerous precision experiments [22–34].

We have performed measurements of the energy gap and impurity concentration in the graphene sample used and compared the experimental mean gradients of the Casimir force with theory based on the first principles of quantum electrodynamics at nonzero temperature with no fitting parameters. For this purpose, the response function of graphene was described by the polarization tensor at nonzero temperature depending on the energy gap and chemical potential which is found in the framework of the Dirac model. The experimental results are in very good agreement with the theoretical ones computed at $T = 294$ K over the entire measurement range within the limits of experimental and theoretical errors. The theoretical gradients of the Casimir force computed using the same theory

with the same experimental parameters at $T = 0$ K are conclusively excluded by the measurement data over the separation region from 250 to 517 nm. Thus, the presence of an unusual thermal effect in graphene systems at short separations is confirmed experimentally.

We have investigated the dependence of the thermal correction to the gradient of the Casimir force between a sphere and a graphene sample, taking into account the values of the energy gap and chemical potential of graphene and also the presence of a substrate. The case of two parallel freestanding sheets of a pristine graphene, originally studied in Ref. [45], was also considered. It was confirmed that an observed size of the thermal effect is in agreement with that for a pristine graphene, taking into account respective decrease due to the presence of a substrate and nonzero values of the energy gap and chemical potential of the graphene sheet used.

An experimental verification of the thermal effect, which is observed in the Casimir interaction with graphene at short separations, offers a clearer view on why a similar effect is experimentally excluded for metallic test bodies. The key point is that for graphene the response function to quantum fluctuations is determined theoretically on the basis of first physical principles. It is nonlocal (i.e., depends both on the frequency and on the wave vector) and pertains equally to quantum fluctuations on the mass shell (the propagating waves) and off the mass shell (the evanescent waves). Then, it is reasonable that the theoretical predictions for the Casimir interaction, which has contributions from both the propagating and evanescent waves, obtained using this formalism are confirmed experimentally. In comparison for metals, their response functions are found partially experimentally from tabulated values [41] and partially using the theoretical extrapolation both given by the effect of only propagating waves. These response functions are reliably tested only in the area of quantum fluctuations on the mass shell. Note that it is even impossible to experimentally test the transverse components of their spatially nonlocal generalizations in the off-mass-shell area [42]. This may be the reason why the Lifshitz theory using the standard Drude model or its generalization for the case of frequency-dependent relaxation parameter (the so-called Gurzhi model) fails to predict the correct values of the Casimir force between metallic test bodies [110].

Thus, information obtained from using graphene leads us to conclude that the Casimir puzzle for metals could be resolved by making the spatially nonlocal modification of the Drude model in the area of evanescent waves which leaves the response to the propagating waves almost unchanged. Such an attempt was already undertaken in Ref. [111]. The suggested spatially nonlocal Drude-like response functions take into account the dissipation properties of conduction electrons, as does the standard Drude model, and simultaneously bring the Lifshitz theory in agreement with measurements of the Casimir force between metallic surfaces. It is pertinent to note that the Lifshitz theory using the nonlocal Drude-like response functions introduced in Ref. [111] satisfies the Nernst heat theorem both for metals with perfect crystal lattices and for lattices with the structural defects [112] (we recall that the Casimir entropy calculated using the standard Drude model violates this fundamental theorem for metals with perfect crystal lattices [35,36,38]).

To conclude, the observation of an unusual thermal effect in graphene systems at short separations, reported in this paper, may stimulate resolution of several other fundamental problems and also be useful for numerous applications of graphene in physics and nanotechnology.

ACKNOWLEDGMENTS

The work of M.L., Y.Z. and U.M. was partially supported by the NSF Grant No. PHY-2012201. The work of G.L.K. and V.M.M. was partially supported by the Peter the

Great Saint Petersburg Polytechnic University in the framework of the Russian state assignment for basic research (Project No. FSEG-2020-0024). V.M.M. was partially funded by the Russian Foundation for Basic Research, Grant No. 19-02-00453 A. His work was also partially supported by the Russian Government Program of Competitive Growth of Kazan Federal University. The authors thank Jianlin Liu, Yongtao Cui, Xiong Huang, Yuan Li, and Yanwei He of the University of California, Riverside for help with and discussions regarding STS.

-
- [1] N. M. R. Peres, The transport properties of graphene: An introduction, *Rev. Mod. Phys.* **82**, 2673 (2010).
- [2] S. Das Sarma, S. Adam, E. H. Hwang, and E. Rossi, Electronic transport in two-dimensional graphene, *Rev. Mod. Phys.* **83**, 407 (2011).
- [3] T. Stauber, N. M. R. Peres, and A. K. Geim, Optical conductivity of graphene in the visible region of the spectrum, *Phys. Rev. B* **78**, 085432 (2008).
- [4] K. F. Mak, M. Y. Sfeir, Y. Wu, C. H. Lui, J. A. Misewich, and T. F. Heinz, Measurement of the Optical Conductivity of Graphene, *Phys. Rev. Lett.* **101**, 196405 (2008).
- [5] M. I. Katsnelson, K. S. Novoselov, and A. K. Geim, Chiral tunnelling and the Klein paradox in graphene, *Nat. Phys.* **2**, 620 (2006).
- [6] D. Allor, T. D. Cohen, and D. A. McGady, Schwinger mechanism and graphene, *Phys. Rev. D* **78**, 096009 (2008).
- [7] C. G. Beneventano, P. Giacconi, E. M. Santangelo, and R. Soldati, Planar QED at finite temperature and density: Hall conductivity, Berry's phases and minimal conductivity of graphene, *J. Phys. A* **42**, 275401 (2009).
- [8] G. L. Klimchitskaya and V. M. Mostepanenko, Creation of quasiparticles in graphene by a time-dependent electric field, *Phys. Rev. D* **87**, 125011 (2013).
- [9] I. Akal, R. Egger, C. Müller, and S. Villarba-Chávez, Low-dimensional approach to pair production in an oscillating electric field: Application to bandgap graphene layers, *Phys. Rev. D* **93**, 116006 (2016).
- [10] M. O. Goerbig, Electronic properties of graphene in a strong magnetic field, *Rev. Mod. Phys.* **83**, 1193 (2011).
- [11] A. H. Castro Neto, F. Guinea, N. M. R. Peres, K. S. Novoselov, and A. K. Geim, The electronic properties of graphene, *Rev. Mod. Phys.* **81**, 109 (2009).
- [12] *Physics of Graphene*, edited by H. Aoki and M. S. Dresselhaus (Springer, Cham, 2014).
- [13] M. I. Katsnelson, *The Physics of Graphene* (Cambridge University Press, Cambridge, 2020).
- [14] H. B. G. Casimir, On the attraction between two perfectly conducting bodies, *Proc. Kon. Ned. Akad. Wet. B* **51**, 793 (1948).
- [15] E. M. Lifshitz, The theory of molecular attractive forces between solids, *Zh. Eksp. Teor. Fiz.* **29**, 94 (1955) [*Sov. Phys. JETP* **2**, 73 (1956)].
- [16] E. M. Lifshitz and L. P. Pitaevskii, *Statistical Physics, Part II* (Pergamon, Oxford, 1980).
- [17] T. Emig, R. L. Jaffe, M. Kardar, and A. Scardicchio, Casimir Interaction Between a Plate and a Cylinder, *Phys. Rev. Lett.* **96**, 080403 (2006).
- [18] M. Bordag, Casimir effect for a sphere and a cylinder in front of a plane and corrections to the proximity force theorem, *Phys. Rev. D* **73**, 125018 (2006).
- [19] O. Kenneth and I. Klich, Casimir forces in a T-operator approach, *Phys. Rev. B* **78**, 014103 (2008).
- [20] T. Emig, N. Graham, R. L. Jaffe, and M. Kardar, Casimir forces between compact objects: The scalar case, *Phys. Rev. D* **77**, 025005 (2008).
- [21] S. J. Rahi, T. Emig, N. Graham, R. L. Jaffe, and M. Kardar, Scattering theory approach to electrodynamic Casimir forces, *Phys. Rev. D* **80**, 085021 (2009).
- [22] R. S. Decca, E. Fischbach, G. L. Klimchitskaya, D. E. Krause, D. López, and V. M. Mostepanenko, Improved tests of extra-dimensional physics and thermal quantum field theory from new Casimir force measurements, *Phys. Rev. D* **68**, 116003 (2003).
- [23] R. S. Decca, D. López, E. Fischbach, G. L. Klimchitskaya, D. E. Krause, and V. M. Mostepanenko, Precise comparison of theory and new experiment for the Casimir force leads to stronger constraints on thermal quantum effects and long-range interactions, *Ann. Phys. (NY)* **318**, 37 (2005).
- [24] R. S. Decca, D. López, E. Fischbach, G. L. Klimchitskaya, D. E. Krause, and V. M. Mostepanenko, Tests of new physics from precise measurements of the Casimir pressure between two gold-coated plates, *Phys. Rev. D* **75**, 077101 (2007).
- [25] R. S. Decca, D. López, E. Fischbach, G. L. Klimchitskaya, D. E. Krause, and V. M. Mostepanenko, Novel constraints on light elementary particles and extra-dimensional physics from the Casimir effect, *Eur. Phys. J. C* **51**, 963 (2007).
- [26] C.-C. Chang, A. A. Banishev, R. Castillo-Garza, G. L. Klimchitskaya, V. M. Mostepanenko, and U. Mohideen, Gradient of the Casimir force between Au surfaces of a sphere and a plate measured using an atomic force microscope in a frequency-shift technique, *Phys. Rev. B* **85**, 165443 (2012).
- [27] A. A. Banishev, C.-C. Chang, G. L. Klimchitskaya, V. M. Mostepanenko, and U. Mohideen, Measurement of the gradient of the Casimir force between a nonmagnetic gold sphere and a magnetic nickel plate, *Phys. Rev. B* **85**, 195422 (2012).
- [28] A. A. Banishev, G. L. Klimchitskaya, V. M. Mostepanenko, and U. Mohideen, Demonstration of the Casimir Force Between Ferromagnetic Surfaces of a Ni-Coated Sphere and a Ni-Coated Plate, *Phys. Rev. Lett.* **110**, 137401 (2013).
- [29] A. A. Banishev, G. L. Klimchitskaya, V. M. Mostepanenko, and U. Mohideen, Casimir force between two magnetic metals in comparison with nonmagnetic test bodies, *Phys. Rev. B* **88**, 155410 (2013).

- [30] G. Bimonte, D. López, and R. S. Decca, Isoelectronic determination of the thermal Casimir force, *Phys. Rev. B* **93**, 184434 (2016).
- [31] J. Xu, G. L. Klimchitskaya, V. M. Mostepanenko, and U. Mohideen, Reducing detrimental electrostatic effects in Casimir-force measurements and Casimir-force-based microdevices, *Phys. Rev. A* **97**, 032501 (2018).
- [32] M. Liu, J. Xu, G. L. Klimchitskaya, V. M. Mostepanenko, and U. Mohideen, Examining the Casimir puzzle with an upgraded AFM-based technique and advanced surface cleaning, *Phys. Rev. B* **100**, 081406(R) (2019).
- [33] M. Liu, J. Xu, G. L. Klimchitskaya, V. M. Mostepanenko, and U. Mohideen, Precision measurements of the gradient of the Casimir force between ultraclean metallic surfaces at larger separations, *Phys. Rev. A* **100**, 052511 (2019).
- [34] G. Bimonte, B. Spreng, P. A. Maia Neto, G.-L. Ingold, G. L. Klimchitskaya, V. M. Mostepanenko, and R. S. Decca, Measurement of the Casimir force between 0.2 and 8 μm : Experimental procedures and comparison with theory, *Universe* **7**, 93 (2021).
- [35] M. Bordag, G. L. Klimchitskaya, U. Mohideen, and V. M. Mostepanenko, *Advances in the Casimir Effect* (Oxford University Press, Oxford, 2015).
- [36] G. L. Klimchitskaya, U. Mohideen, and V. M. Mostepanenko, The Casimir force between real materials: Experiment and theory, *Rev. Mod. Phys.* **81**, 1827 (2009).
- [37] L. M. Woods, D. A. R. Dalvit, A. Tkatchenko, P. Rodriguez-Lopez, A. W. Rodriguez, and R. Podgornik, Materials perspective on Casimir and van der Waals interactions, *Rev. Mod. Phys.* **88**, 045003 (2016).
- [38] V. M. Mostepanenko, Casimir puzzle and Casimir conundrum: Discovery and search for resolution, *Universe* **7**, 84 (2021).
- [39] A. O. Sushkov, W. J. Kim, D. A. R. Dalvit, and S. K. Lamoreaux, Observation of the thermal Casimir force, *Nat. Phys.* **7**, 230 (2011).
- [40] V. B. Bezerra, G. L. Klimchitskaya, U. Mohideen, V. M. Mostepanenko, and C. Romero, Impact of surface imperfections on the Casimir force for lenses of centimeter-size curvature radii, *Phys. Rev. B* **83**, 075417 (2011).
- [41] *Handbook of Optical Constants of Solids*, edited by E. D. Palik (Academic Press, New York, 1985).
- [42] M. Dressel and G. Grüner, *Electrodynamics of Solids: Optical Properties of Electrons in Metals* (Cambridge University Press, Cambridge, 2003).
- [43] M. Boström and Bo E. Sernelius, Thermal Effects on the Casimir Force in the 0.1–5 μm range, *Phys. Rev. Lett.* **84**, 4757 (2000).
- [44] J. F. Dobson, A. White, and A. Rubio, Asymptotics of the Dispersion Interaction: Analytic Benchmarks for Van Der Waals Energy Functionals, *Phys. Rev. Lett.* **96**, 073201 (2006).
- [45] G. Gómez-Santos, Thermal van der Waals interaction between graphene layers, *Phys. Rev. B* **80**, 245424 (2009).
- [46] D. Drosdoff and L. M. Woods, Casimir forces and graphene sheets, *Phys. Rev. B* **82**, 155459 (2010).
- [47] D. Drosdoff and L. M. Woods, Casimir interaction between graphene sheets and metamaterials, *Phys. Rev. A* **84**, 062501 (2011).
- [48] Bo E. Sernelius, Casimir interactions in graphene systems, *Europhys. Lett.* **95**, 57003 (2011).
- [49] T. E. Judd, R. G. Scott, A. M. Martin, B. Kaczmarek, and T. M. Fromhold, Quantum reflection of ultracold atoms from thin films, graphene and semiconductor heterostructures, *New J. Phys.* **13**, 083020 (2011).
- [50] J. Sarabadani, A. Naji, R. Asgari, and R. Podgornik, Many-body effects in the van der Waals-Casimir interaction between graphene layers, *Phys. Rev. B* **84**, 155407 (2011); **87**, 239905(E) (2013).
- [51] D. Drosdoff, A. D. Phan, L. M. Woods, I. V. Bondarev, and J. F. Dobson, Effects of spatial dispersion on the Casimir force between graphene sheets, *Eur. Phys. J. B* **85**, 365 (2012).
- [52] Bo E. Sernelius, Retarded interactions in graphene systems, *Phys. Rev. B* **85**, 195427 (2012); **89**, 079901(E) (2014).
- [53] W.-K. Tse and A. H. MacDonald, Quantized Casimir Force, *Phys. Rev. Lett.* **109**, 236806 (2012).
- [54] A. D. Phan, L. M. Woods, D. Drosdoff, I. V. Bondarev, and N. A. Viet, Temperature dependent graphene suspension due to thermal Casimir interaction, *Appl. Phys. Lett.* **101**, 113118 (2012).
- [55] A. D. Phan, N. A. Viet, N. A. Poklonski, L. M. Woods, and C. H. Le, Interaction of a graphene sheet with a ferromagnetic metal plate, *Phys. Rev. B* **86**, 155419 (2012).
- [56] S. Ribeiro and S. Scheel, Shielding vacuum fluctuations with graphene, *Phys. Rev. A* **88**, 042519 (2013); **89**, 039904(E) (2014).
- [57] T. Cysne, W. J. M. Kort-Kamp, D. Oliver, F. A. Pinheiro, F. S. S. Rosa, and C. Farina, Tuning the Casimir-Polder interaction via magneto-optical effects in graphene, *Phys. Rev. A* **90**, 052511 (2014).
- [58] N. Knusnutdinov, R. Kashapov, and L. M. Woods, Casimir-Polder effect for a stack of conductive planes, *Phys. Rev. A* **94**, 012513 (2016).
- [59] N. Inui, Casimir effect on graphene resonator, *J. Appl. Phys.* **119**, 104502 (2016).
- [60] N. Knusnutdinov, R. Kashapov, and L. M. Woods, Thermal Casimir and Casimir-Polder interactions in N parallel 2D Dirac materials, *2D Materials* **5**, 035032 (2018).
- [61] A. Derras-Chouk, E. M. Chudnovsky, D. A. Garanin, and R. Jaafar, Graphene cantilever under Casimir force, *J. Phys. D: Appl. Phys.* **51**, 195301 (2018).
- [62] P. K. Pyatkovsky, Dynamical polarization, screening, and plasmons in gapped graphene, *J. Phys.: Condens. Matter* **21**, 025506 (2009).
- [63] M. Bordag, I. V. Fialkovsky, D. M. Gitman, and D. V. Vassilevich, Casimir interaction between a perfect conductor and graphene described by the Dirac model, *Phys. Rev. B* **80**, 245406 (2009).
- [64] I. V. Fialkovsky, V. N. Marachevsky, and D. V. Vassilevich, Finite-temperature Casimir effect for graphene, *Phys. Rev. B* **84**, 035446 (2011).
- [65] M. Bordag, G. L. Klimchitskaya, V. M. Mostepanenko, and V. M. Petrov, Quantum field theoretical description for the reflectivity of graphene, *Phys. Rev. D* **91**, 045037 (2015); **93**, 089907(E) (2016).
- [66] M. Bordag, I. Fialkovskiy, and D. Vassilevich, Enhanced Casimir effect for doped graphene, *Phys. Rev. B* **93**, 075414 (2016); **95**, 119905(E) (2017).
- [67] M. Bordag, G. L. Klimchitskaya, and V. M. Mostepanenko, Thermal Casimir effect in the interaction of graphene with dielectrics and metals, *Phys. Rev. B* **86**, 165429 (2012).

- [68] M. Chaichian, G. L. Klimchitskaya, V. M. Mostepanenko, and A. Tureanu, Thermal Casimir-Polder interaction of different atoms with graphene, *Phys. Rev. A* **86**, 012515 (2012).
- [69] G. L. Klimchitskaya and V. M. Mostepanenko, Van der Waals and Casimir interactions between two graphene sheets, *Phys. Rev. B* **87**, 075439 (2013).
- [70] B. Arora, H. Kaur, and B. K. Sahoo, C_3 coefficients for the alkali atoms interacting with a graphene and carbon nanotube, *J. Phys. B* **47**, 155002 (2014).
- [71] K. Kaur, J. Kaur, B. Arora, and B. K. Sahoo, Emending thermal dispersion interaction of Li, Na, K and Rb alkali-metal atoms with graphene in the Dirac model, *Phys. Rev. B* **90**, 245405 (2014).
- [72] G. L. Klimchitskaya and V. M. Mostepanenko, Classical Casimir-Polder force between polarizable microparticles and thin films including graphene, *Phys. Rev. A* **89**, 012516 (2014).
- [73] G. L. Klimchitskaya and V. M. Mostepanenko, Classical limit of the Casimir interaction for thin films with applications to graphene, *Phys. Rev. B* **89**, 035407 (2014).
- [74] G. L. Klimchitskaya and V. M. Mostepanenko, Observability of thermal effects in the Casimir interaction from graphene-coated substrates, *Phys. Rev. A* **89**, 052512 (2014).
- [75] G. L. Klimchitskaya and V. M. Mostepanenko, Impact of graphene coating on the atom-plate interaction, *Phys. Rev. A* **89**, 062508 (2014).
- [76] G. L. Klimchitskaya, V. M. Mostepanenko, and Bo E. Sernelius, Two approaches for describing the Casimir interaction with graphene: Density-density correlation function versus polarization tensor, *Phys. Rev. B* **89**, 125407 (2014).
- [77] G. L. Klimchitskaya and V. M. Mostepanenko, Origin of large thermal effect in the Casimir interaction between two graphene sheets, *Phys. Rev. B* **91**, 174501 (2015).
- [78] G. Bimonte, G. L. Klimchitskaya, and V. M. Mostepanenko, How to observe the giant thermal effect in the Casimir force for graphene systems, *Phys. Rev. A* **96**, 012517 (2017).
- [79] G. Bimonte, G. L. Klimchitskaya, and V. M. Mostepanenko, Thermal effect in the Casimir force for graphene and graphene-coated substrates: Impact of nonzero mass gap and chemical potential, *Phys. Rev. B* **96**, 115430 (2017).
- [80] C. Henkel, G. L. Klimchitskaya, and V. M. Mostepanenko, Influence of chemical potential on the Casimir-Polder interaction between an atom and gapped graphene or graphene-coated substrate, *Phys. Rev. A* **97**, 032504 (2018).
- [81] A. A. Banishev, H. Wen, J. Xu, R. K. Kawakami, G. L. Klimchitskaya, V. M. Mostepanenko, and U. Mohideen, Measuring of the Casimir force gradient from graphene on a SiO₂ substrate, *Phys. Rev. B* **87**, 205433 (2013).
- [82] G. L. Klimchitskaya, U. Mohideen, and V. M. Mostepanenko, Theory of the Casimir interaction for graphene-coated substrates using the polarization tensor and comparison with experiment, *Phys. Rev. B* **89**, 115419 (2014).
- [83] M. Liu, Y. Zhang, G. L. Klimchitskaya, V. M. Mostepanenko, and U. Mohideen, Demonstration of Unusual Thermal Effect in the Casimir Force from Graphene, *Phys. Rev. Lett.* **126**, 206802 (2021).
- [84] Grollttx, San Diego, CA, <http://www.grollttx.com>
- [85] MSE Supplies, Tucson, AZ, <http://www.msesupplies.com>
- [86] Y. Wang, Y. Zheng, X. Xu, E. Dubuisson, Q. Bao, J. Lu, and K. Ping Loh, Electrochemical delamination of CVD-grown graphene film: Toward the recyclable use of copper catalyst, *ACS Nano* **5**, 9927 (2011).
- [87] HQ: CSC38/tipless, MicroMash, Watsonville, CA, <http://www.nanoandmore.com>
- [88] F. J. Giessibl, Advances in atomic force microscopy, *Rev. Mod. Phys.* **75**, 949 (2003).
- [89] R. O. Behunin, D. A. R. Dalvit, R. S. Decca, C. Genet, I. W. Jung, A. Lambrecht, A. Liscio, D. López, S. Reynaud, G. Schnoering, G. Voisin, and Y. Zeng, Kelvin probe force microscopy of metallic surfaces used in Casimir force measurements, *Phys. Rev. A* **90**, 062115 (2014).
- [90] J. L. Garrett, J. Kim, and J. N. Munday, Measuring the effect of electrostatic patch potentials in Casimir force experiments, *Phys. Rev. Res.* **2**, 023355 (2020).
- [91] A. Das, S. Pisana, B. Chakraborty, S. Piscanec, S. K. Saha, U. V. Waghmare, K. S. Novoselov, H. R. Krishnamurthy, A. K. Geim, A. C. Ferrari, and A. K. Sood, Monitoring dopants by Raman scattering in an electrochemically top-gated graphene transistor, *Nature Nanotech.* **3**, 210 (2008).
- [92] L. A. Falkovsky, Optical properties of graphene, *J. Phys.: Conf. Series* **129**, 012004 (2008).
- [93] L. A. Falkovsky, Thermodynamics of electron-hole liquids in graphene, *Pis'ma v ZhETF* **98**, 183 (2013) [*JETP Lett.* **98**, 161 (2013)].
- [94] G. Li, A. Luican, and E. Y. Andrei, Scanning Tunneling Spectroscopy of Graphene on Graphite, *Phys. Rev. Lett.* **102**, 176804 (2009).
- [95] Y. Zhang, V. W. Brar, C. Girit, A. Zettl, and M. F. Crommie, Origin of spatial charge inhomogeneity in graphene, *Nat. Phys.* **5**, 722 (2009).
- [96] J. Martin, N. Akerman, G. Ulbricht, T. Lohmann, J. H. Smet, K. von Klitzing, and A. Yacoby, Observation of electron-hole puddles in graphene using a scanning single-electron transistor, *Nat. Phys.* **4**, 144 (2008).
- [97] M. L. Teague, A. P. Lai, J. Velasco, C. R. Hughes, A. D. Beyer, M. W. Bockrath, C. N. Lau, and N.-C. Yeh, Evidence for strain-induced local conductance modulations in single-layer graphene on SiO₂, *Nano Lett.* **9**, 2542 (2009).
- [98] V. Geringer, M. Liebmann, T. Echtermeyer, S. Runte, M. Schmidt, R. Rückamp, M. C. Lemme, and M. Morgenstern, Intrinsic and Extrinsic Corrugation of Monolayer Graphene Deposited on SiO₂, *Phys. Rev. Lett.* **102**, 076102 (2009).
- [99] L. Huder, A. Artaud, T. Le Quang, G. T. de Laissardière, A. G. M. Jansen, G. Lapertot, C. Chapelier, and V. T. Renard, Electronic Spectrum of Twisted Graphene Layers Under Heterostrain, *Phys. Rev. Lett.* **120**, 156405 (2018).
- [100] E. Y. Andrei, G. Li, and X. Du, Electronic properties of graphene: A perspective from scanning tunneling microscopy and magnetotransport, *Rep. Progr. Phys.* **75**, 056501 (2012).
- [101] T. Zhu, M. Antezza, and J.-S. Wang, Dynamical polarizability of graphene with spatial dispersion, *Phys. Rev. B* **103**, 125421 (2021).
- [102] M. Bordag, G. L. Klimchitskaya, and V. M. Mostepanenko, The Casimir force between plates with small deviations from plane-parallel geometry, *Int. J. Mod. Phys. A* **10**, 2661 (1995).
- [103] P. J. van Zwol, G. Palasantzas, and J. Th. M. De Hosson, Influence of random roughness on the Casimir force at small separations, *Phys. Rev. B* **77**, 075412 (2008).

- [104] S. de Man, K. Heeck, and D. Iannuzzi, Halving the Casimir force with conductive oxides: Experimental details, *Phys. Rev. A* **82**, 062512 (2010).
- [105] C. D. Fosco, F. C. Lombardo, and F. D. Mazzitelli, Proximity force approximation for the Casimir energy as a derivative expansion, *Phys. Rev. D* **84**, 105031 (2011).
- [106] G. Bimonte, T. Emig, R. L. Jaffe, and M. Kardar, Casimir forces beyond the proximity force approximation, *Europhys. Lett.* **97**, 50001 (2012).
- [107] G. Bimonte, T. Emig, and M. Kardar, Material dependence of Casimir force: Gradient expansion beyond proximity, *Appl. Phys. Lett.* **100**, 074110 (2012).
- [108] G. Bimonte, Going beyond PFA: A precise formula for the sphere-plate Casimir force, *Europhys. Lett.* **118**, 20002 (2017).
- [109] M. Hartmann, G.-L. Ingold, and P. A. Maia Neto, Plasma Versus Drude Modeling of the Casimir Force: Beyond the Proximity Force Approximation, *Phys. Rev. Lett.* **119**, 043901 (2017).
- [110] G. L. Klimchitskaya, V. M. Mostepanenko, Kailiang Yu, and L. M. Woods, Casimir force, causality, and the Gurzhi model, *Phys. Rev. B* **101**, 075418 (2020).
- [111] G. L. Klimchitskaya and V. M. Mostepanenko, An alternative response to the off-shell quantum fluctuations: A step forward in resolution of the Casimir puzzle, *Eur. Phys. J. C* **80**, 900 (2020).
- [112] G. L. Klimchitskaya and V. M. Mostepanenko, Casimir entropy and nonlocal response functions to the off-shell quantum fluctuations, *Phys. Rev. D* **103**, 096007 (2021).